*Work supported in part by the U. S. Atomic Energy Commission.

†Permanent address.

[1]V. V. Ammosov *et al.*, Phys. Lett. 42B, 519 (1972); J. W. Chapman *et al.*, Phys. Rev. Lett. 29, 1686 (1972); G. Charlton *et al.*, *ibid.* 29, 515 (1972); F. T. Dao *et al.*, *ibid.* 29, 1627 (1972).

[2]G. D. Kaiser, Nucl. Phys. B44, 171 (1972); DNPL Report Nos. DNPL/P 125, 1972; DNPL/P 148, 1973 (unpublished).

[3]G. W. Parry and P. Rotelli, ICTP Trieste Report No. IC/73/3, 1973 (unpublished).

[4]Y. Tomozawa, Nucl. Phys. B (to be published).

[5]W. Frazer *et al.*, Rev. Mod. Phys. 44, 284 (1972) and references quoted therein.

[6]E.g., S.-J. Chang, T.-M. Yan, and Y.-P. Yao, Phys. Rev. D 4, 3019 (1971).

[7]E.g., T. D. Lee, Phys. Rev. D 6, 3617 (1972).

[8]H. Cramér, *Mathematical Methods of Statistics* (Princeton Univ. Press, Princeton, N. J., 1946).

[9]M. G. Kendall and A. Stuart, *The Advanced Study of Statistics* (Griffin, London, 1963), Vol. 1.

[10]B. R. Webber, Phys. Lett. 42B, 69 (1972).

[11]A. H. Mueller, Phys. Rev. D 4, 150 (1971).

[12]In Ref. 9, μ_k' and μ_k are used for moments and dispersion moments.

[13]J. B. S. Haldane, Biometrika 32, 294 (1942).

[14]For more elaborate models of this sort, see S. Barshay, Phys. Lett. 42B, 457 (1972); H. B. Nielsen and P. Olesen, Phys. Lett. 43B, 37 (1973). Also see exercise 3.23 in Ref. 9.

[15]I. S. Gradshteyn and I. M. Ryzhik, *Tables of Integrals, Series and Products* (Academic, New York, 1965), p. 46; Jahnke, Emde, and Lösch, *Tables of Higher Functions* (McGraw-Hill, New York, 1960), p. 298.

[16]C. Quigg and J. D. Jackson, NAL Report No. NAL-THY-93, 1972 (unpublished).

[17]Z. Koba, H. B. Nielsen, and P. Olesen, Nucl. Phys. B40, 317 (1972).

[18]P. Slattery, Phys. Rev. D 7, 2073 (1973).

[19]P. Olesen, Phys. Lett. 41B, 602 (1972).

[20]W. I. Weisberger, report, 1973 (unpublished).

[21]Equation (4.7) is called the Edgeworth form of the Type-A series; see F. Y. Edgeworth, Trans. Camb. Phil. Soc. 20, 36 (1904); 20, 113 (1904); Ref. 9, p. 157.

[22]E. A. Cornish and R. A. Fisher, Rev. Inst. Int. Statist. 5, 307 (1937); Technometrics 2, 209 (1960); Ref. 9, Eq. (6.49).

PHYSICAL REVIEW D VOLUME 8, NUMBER 7 1 OCTOBER 1973

Unified Model of Current-Hadronic Interactions*

J. W. Moffat and A. C. D. Wright

Department of Physics, University of Toronto, Toronto, Canada

(Received 18 June 1973)

A model for current-hadronic interactions is constructed which satisfies (a) Mandelstam analyticity, (b) crossing symmetry, (c) scale invariance in the deep-inelastic region, (d) Regge behavior in all channels, (e) resonance poles in the unphysical sheet, (f) generalized vector-meson dominance, and (g) SU(3) structure of the currents. There is a fixed pole in the charged photon-proton scattering amplitude, so that the Dashen–Fubini–Gell-Mann and Adler sum rules are satisfied. Good fits are obtained for Compton scattering at energies above 5 GeV for all experimentally available values of $-q^2$, and also for all deep-inelastic electroproduction data. By fixing all parameters with these fits, and with preliminary data obtained from deep-inelastic experiments on production by neutrinos, we are able to make parameter-free predictions of ρ^0 and ω^0 photoproduction and electroproduction, which agree well with the data.

I. INTRODUCTION

Bjorken's[1] observation that the inclusive electroproduction and neutrino-scattering structure functions might obey a simple scale-invariance law in the deep-inelastic region and the experimental investigations of this proposal[2,3] have stimulated much theoretical work in the past few years. Some models, such as the parton model[4] and the related light-cone algebras,[5] attempt to explain the scale invariance on the basis of an underlying constituent structure of the proton. Another approach is to take scale invariance as given, and to concentrate on satisfying additional fundamental requirements. Although the division between the two approaches is ill defined, we might include various Regge,[6,7] dual,[8] and vector-dominance[9] models in the second category.

In this paper we present a model for inclusive electroproduction, Compton scattering, neutrino scattering, photoproduction, and electroproduction of vector mesons from a nucleon. The essential feature of the model is Mandelstam analyticity, which is obtained by extending an analytic, crossing-symmetric K-π amplitude[10,11] to the case where two of the external legs are off-mass-shell currents. Within this framework, we find it possible to incorporate Bjorken scale invariance and

vector-meson dominance. The model possesses Regge behavior in all channels and resonances in the direct channels; the correct crossing properties are also incorporated. A discussion of the Adler sum rule in our model shows that it cannot be accounted for by the Regge part, but must arise from the Dashen–Fubini–Gell-Mann[12] fixed pole.

We obtain good fits to the scale-invariant electroproduction structure functions F_2^p and F_2^n, as well as the difference $\Delta F_2 \equiv (F_2^p - F_2^n)$, which is important for the proton-neutron mass difference,[13] and the ratio $R \equiv F_2^n/F_2^p$. We simultaneously fit the total Compton cross section $\sigma(\gamma p)$ and the scale-invariant neutrino-scattering function $(F_2^{\bar{\nu}p} + F_2^{\nu p})$ on the assumption that the vector and axial-vector currents contribute equally in the scale-invariant limit. Our results are consistent with the preliminary data from the CERN bubble-chamber experiment.[14]

We find that νW_2 must contain a q^2-dependent function which corrects the q^2 behavior of the vector-meson propagator, thereby allowing reasonable fits to the scale-breaking behavior of νW_2. Once this is fixed for inclusive electroproduction, we obtain parameter-free predictions for the photoproduction and electroproduction of ρ^0 and ω^0 mesons, which are in excellent agreement with experiment.

The plan of the paper is as follows. In Sec. II we discuss notation, kinematics, and scattering amplitudes. Section III treats the crossing and isospin properties of the invariant amplitude. Our model for the amplitude T_2 is presented in Sec. IV, along with a discussion of its features and applications to electroproduction, neutrino scattering, Compton scattering, and vector-meson photoproduction, and electroproduction. Section V deals with the Dashen–Fubini–Gell-Mann and Adler sum rules. We describe our fits to experimental data and predictions for vector-meson photoproduction and electroproduction in Sec. VI, and summarize our work in Sec. VII.

II. NOTATION AND KINEMATICS

We consider the scattering of a vector boson off a nucleon of mass M. For simplicity, we treat the nucleon as spinless. This is physically reasonable for the structure functions, which are spin-averaged, and at high energy for photoproduction and electroproduction. Our process is $B_1(q_1) + N(p_1) \to B_2(q_2) + N(p_2)$.

The invariant T matrix is connected to the S matrix by

$$S_{fi} = \delta_{fi} + i(2\pi)^4 \delta^4(q_2 + p_2 - q_1 - p_1) T_{fi}\,, \tag{2.1}$$

and, in the c.m. system, the differential cross section is

$$\frac{d\sigma}{d\Omega} = \frac{q'}{q} |f(q,\theta)|^2\,, \tag{2.2}$$

where

$$f(q,\theta) = \frac{16\pi^5 M T}{\sqrt{s}}\,, \tag{2.3}$$

and q and q' are the initial and final c.m. momenta. The Mandelstam variables are

$$\begin{aligned} s &= (q_1 + p_1)^2 = (q_2 + p_2)^2\,, \\ t &= (q_1 - q_2)^2 = (p_1 - p_2)^2\,, \\ u &= (q_1 - p_2)^2 = (p_1 - q_2)^2\,. \end{aligned} \tag{2.4}$$

The variables s, t, and u satisfy the relation

$$s + t + u = 2M^2 + q_1^2 + q_2^2\,. \tag{2.5}$$

From (2.2) and (2.3), we have

$$\frac{d\sigma}{d\Omega} = \frac{(2\pi)^{10} M^2}{4s} \frac{q'}{q} |T|^2\,. \tag{2.6}$$

The covariant current correlation function for the two-current process shown in Fig. 1 is given by

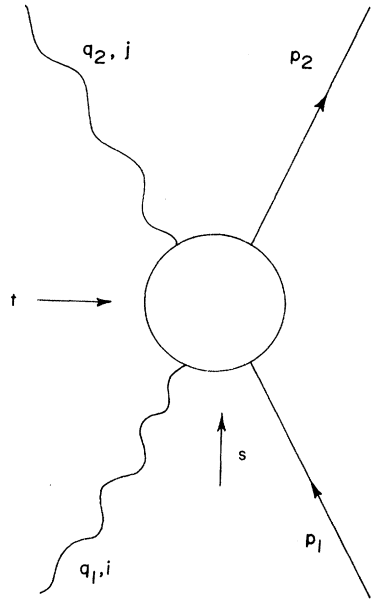

FIG. 1. Definition of kinematic variables for current-nucleon scattering.

$$T_{\mu\nu}^{*ij}(q_2, p_2; q_1, p_1) = i(2\pi)^3 \int d^4x\, e^{iq_2 \cdot x} \theta(x^0) \langle p_2 | [\, V_\mu^j(x), V_\nu^i(0)] \, | p_1 \rangle + (\text{polynomials in } q)\,, \tag{2.7}$$

where the $V_\mu^i(x)$ $(i=1,\ldots,8)$ form an SU(3) octet of vector currents and the hadron target is assumed to be a proton, unless otherwise indicated.

We also define the electromagnetic amplitude

$$T^*_{\mu\nu}(q_2,p_2;q_1,p_1)=i(2\pi)^3\int d^4x\, e^{iq_2\cdot x}\theta(x^0)\langle p_2|[J^{\rm em}_\mu(x),J^{\rm em}_\nu(0)]\,|p_1\rangle+(\text{polynomials in } q) \tag{2.8}$$

and the weak amplitude

$$T^{*(\bar\nu,\nu)}_{\mu\nu}(q_2,p_2;q_1,p_1)=i(2\pi)^3\int d^4x\, e^{iq_2\cdot x}\theta(x^0)\langle p_2|[J^{\pm}_\mu(x),J^{\mp}_\nu(0)]\,|p_1\rangle+(\text{polynomials in } q). \tag{2.9}$$

Here we assume that the hadronic electromagnetic current is given by

$$J^{\rm em}_\mu(x)=V^3_\mu(x)+\frac{1}{\sqrt{3}}V^8_\mu(x). \tag{2.10}$$

We also assume that $\sin^2\theta_C$ is negligible, where θ_C is the Cabibbo angle, so that

$$J^{\pm}_\mu(x)=J^1_\mu(x)\pm iJ^2_\mu(x), \tag{2.11}$$

where

$$J^i_\mu(x)=V^i_\mu(x)-A^i_\mu(x), \tag{2.12}$$

and $A^i_\mu(x)$ $(i=1,\ldots,8)$ form an octet of axial-vector currents.

The amplitude $T^{*ij}_{\mu\nu}$ may be expanded in kinematic-zero- and singularity-free amplitudes. Assuming parity conservation, we have

$$\begin{aligned}T^{*ij}_{\mu\nu}=&-T^{ij}_1 g_{\mu\nu}+T^{ij}_2\frac{P_\mu P_\nu}{M^2}+T^{ij}_3 Q_\mu Q_\nu\\&+T^{ij}_4 Q_\mu P_\nu+T^{ij}_5 P_\mu Q_\nu+T^{ij}_6 Q_\mu\Delta_\nu\\&+T^{ij}_7\Delta_\mu Q_\nu+T^{ij}_8 P_\mu\Delta_\nu+T^{ij}_9\Delta_\mu P_\nu\\&+T^{ij}_{10}\Delta_\mu\Delta_\nu,\end{aligned} \tag{2.13}$$

where

$$\begin{aligned}P&=\tfrac12(p_1+p_2),\\Q&=\tfrac12(q_1+q_2),\\\Delta&=(q_1-q_2).\end{aligned} \tag{2.14}$$

The T^{ij}_k $(k=1,\ldots,10)$ are functions of the kinematic invariants

$$T^{ij}_k=T^{ij}_k(s,t,q_1^2,q_2^2). \tag{2.15}$$

Time-reversal invariance gives the result

$$\begin{aligned}T^{ij}_1(s,t,q_1^2,q_2^2)&=T^{ji}_1(s,t,q_2^2,q_1^2),\\T^{ij}_2(s,t,q_1^2,q_2^2)&=T^{ji}_2(s,t,q_2^2,q_1^2).\end{aligned} \tag{2.16}$$

The amplitudes $T^*_{\mu\nu}$ and $T^{*(\bar\nu,\nu)}_{\mu\nu}$ may also be expanded in invariant amplitudes:

$$T^*_{\mu\nu}=-T_1 g_{\mu\nu}+T_2\frac{P_\mu P_\nu}{M^2}+\cdots, \tag{2.17}$$

$$T^{*(\bar\nu,\nu)}_{\mu\nu}=-T^{(\bar\nu,\nu)}_1 g_{\mu\nu}+T^{(\bar\nu,\nu)}_2\frac{P_\mu P_\nu}{M^2}+iT^{(\bar\nu,\nu)}_3\epsilon_{\mu\nu\sigma\tau}P^\sigma Q^\tau/2M^2+\cdots. \tag{2.18}$$

Hence, (2.10) gives

$$T_2=T^{33}_2+\frac{1}{\sqrt3}T^{38}_2+\frac{1}{\sqrt3}T^{83}_2+\tfrac13 T^{88}_2, \tag{2.19}$$

and similarly for T_1.

The gauge condition for $T^*_{\mu\nu}$ is

$$q_1^\nu T^*_{\mu\nu}=q_2^\mu T^*_{\mu\nu}=0. \tag{2.20}$$

At $\Delta=0$ this gives the usual gauge-invariant decomposition

$$\begin{aligned}T^*_{\mu\nu}(q,p;q,p)=&-\left(g_{\mu\nu}-\frac{q_\mu q_\nu}{q^2}\right)T_1(s,0,q^2,q^2)\\&+\frac{1}{M^2}\left(p_\mu-\frac{p\cdot q}{q^2}q_\mu\right)\left(p_\nu-\frac{p\cdot q}{q^2}q_\nu\right)\\&\times T_2(s,0,q^2,q^2).\end{aligned} \tag{2.21}$$

We require (2.17) to reduce at $q_1^2=q_2^2=0$ to the gauge-invariant form[15]

$$\begin{aligned}M_{\mu\nu}=&-[(q_1\cdot q_2)g_{\mu\nu}-q_{1\mu}q_{2\nu}]B_1\\&+\frac{1}{M^2}[(q_1\cdot q_2)P_\mu P_\nu+(P\cdot Q)^2 g_{\mu\nu}\\&-(P\cdot Q)(q_{1\mu}P_\nu+P_\mu q_{2\nu})]B_2,\end{aligned} \tag{2.22}$$

which is the physical Compton amplitude. This gives

$$T_2=(q_1\cdot q_2)B_2 \tag{2.23}$$

at $q^2=0$. We therefore adopt the general form

$$\begin{aligned}T_2(s,t,q_1^2,q_2^2)=&-(q_1\cdot q_2)A(s,t,q_1^2,q_2^2)\\&+B(s,t,q_1^2,q_2^2),\end{aligned} \tag{2.24}$$

where B is the Born term. We assume that A is free of kinematic zeros and singularities, and satisfies a Mandelstam representation.

By (2.12), we can write, in an obvious notation,

$$\begin{aligned}T^{(\bar\nu,\nu)}_1&=T^{(\bar\nu,\nu)}_{1V}+T^{(\bar\nu,\nu)}_{1A},\\T^{(\bar\nu,\nu)}_2&=T^{(\bar\nu,\nu)}_{2V}+T^{(\bar\nu,\nu)}_{2A}.\end{aligned} \tag{2.25}$$

The gauge condition for $T_{2V}^{(\bar{\nu},\nu)}$ is[16]

$$T_{2V}^{(\bar{\nu},\nu)}(s,t,0,t)=T_{2V}^{(\bar{\nu},\nu)}(s,t,t,0)=\mp\frac{4MF_V(t)}{s-M^2}, \tag{2.26}$$

where $F_V(t)$ is the isovector form factor which satisfies $F_V(0)=\frac{1}{2}$. Hence, we write in general

$$T_{2V}^{(\bar{\nu},\nu)}(s,t,q_1^2,q_2^2)=-(q_1\cdot q_2)A_V^{(\bar{\nu},\nu)}(s,t,q_1^2,q_2^2)+F^{(\bar{\nu},\nu)}(s,t,q_1^2,q_2^2), \tag{2.27}$$

where F is the fixed-pole term (which contains the Born term). We see that (2.26) is satisfied when

$$F^{(\bar{\nu},\nu)}(s,t,0,t)=F^{(\bar{\nu},\nu)}(s,t,t,0)=\mp\frac{4MF_V(t)}{s-M^2}. \tag{2.28}$$

For the general amplitude T_2^{ij} we have

$$T_2^{ij}(s,t,q_1^2,q_2^2)=-(q_1\cdot q_2)A_{ij}(s,t,q_1^2,q_2^2)+C_{ij}(s,t,q_1^2,q_2^2), \tag{2.29}$$

where C_{ij} contains the Born term and fixed pole, and A_{ij} is assumed to have a Mandelstam representation. For T_1^{ij}, we generalize the Compton relation[6]

$$T_1(\nu,q^2)=-\frac{\nu^2}{q^2}T_2(\nu,q^2), \tag{2.30}$$

to

$$T_1^{ij}(s,t,q_1^2,q_2^2)=-\frac{(P\cdot Q)^2}{M^2(q_1\cdot q_2)}T_2^{ij}(s,t,q_1^2,q_2^2). \tag{2.31}$$

The spin-dependent Compton differential cross section is given by (2.6),[16a] with

$$T(s,t,q_1^2,q_2^2)=\frac{e^2}{(2\pi)^6}\epsilon_2^{\mu *}\epsilon_1^{\nu}T_{\mu\nu}^*(q_2,p_2;q_1,p_1), \tag{2.32}$$

where ϵ_1^{μ} and ϵ_2^{μ} are the polarization vectors of the incoming and outgoing photon, respectively, and $T_{\mu\nu}^*$ is defined in (2.8). Using (2.30), the unpolarized cross section at $\Delta=0$ reads

$$\frac{d\sigma}{dt}=\frac{\pi M^2\alpha^2}{sqq'}\left[\frac{(p\cdot q)^4}{M^4q^4}+\frac{1}{2}\right]|T_2|^2. \tag{2.33}$$

A simple generalization is

$$\frac{d\sigma}{dt}=\frac{\pi M^2\alpha^2}{sqq'}\left[\frac{(P\cdot Q)^4}{M^4(q_1\cdot q_2)^2}+\frac{1}{2}\right]|T_2|^2, \tag{2.34}$$

which we assume to hold for small $|t|\neq 0$.

The electroproduction structure functions are defined by

$$W_i(\nu,q^2)=\frac{1}{\pi}\operatorname{Im}T_i(s,0,q^2,q^2)\quad(i=1,2), \tag{2.35}$$

where $\nu=p\cdot q/M$. Then the cross section for inclusive electroproduction $e+p\to e+$ hadrons is given by

$$\frac{d^2\sigma}{d\Omega dE'}=\left(\frac{d\sigma}{d\Omega}\right)_{\text{Mott}}[W_2(\nu,q^2)+2W_1(\nu,q^2)\tan^2(\tfrac{1}{2}\theta)]. \tag{2.36}$$

Here E' is the energy of the outgoing electron in the lab frame, and θ is the lab scattering angle. Also,

$$\left(\frac{d\sigma}{d\Omega}\right)_{\text{Mott}}=\left(\frac{4\alpha^2}{q^4}\right)E'^2\cos^2(\tfrac{1}{2}\theta). \tag{2.37}$$

In terms of the photoabsorption cross sections of longitudinal and transverse virtual photons σ_S and σ_T, we have

$$W_1(\nu,q^2)=\frac{1}{4\pi^2\alpha}\left(\nu+\frac{q^2}{2M}\right)\sigma_T, \tag{2.38}$$

$$\nu W_2(\nu,q^2)=\frac{1}{4\pi^2\alpha}\left(1+\frac{q^2}{2M\nu}\right)|q^2|\left(\frac{\sigma_T+\sigma_S}{1-q^2/\nu^2}\right).$$

The real photoabsorption cross section reads

$$\sigma(\gamma N)=\lim_{q^2\to 0}\frac{4\pi^2\alpha}{|q^2|}[\nu W_2(\nu,q^2)]. \tag{2.39}$$

Finally, the cross sections for the inclusive processes

$$\bar{\nu}_l+p\to\bar{l}+\text{hadrons},\qquad(l=e\text{ or }\mu)$$
$$\nu_l+p\to l+\text{hadrons}$$

are given by

$$\frac{d\sigma^{(\bar{\nu},\nu)}}{d\Omega dE'}=\frac{G^2E'^2}{2\pi^2}\left[W_2^{(\bar{\nu},\nu)}(\nu,q^2)\cos^2(\tfrac{1}{2}\theta)+2W_1^{(\bar{\nu},\nu)}(\nu,q^2)\sin^2(\tfrac{1}{2}\theta)\pm W_3^{(\bar{\nu},\nu)}(\nu,q^2)\sin^2(\tfrac{1}{2}\theta)\left(\frac{E+E'}{M}\right)\right], \tag{2.40}$$

where

$$W_i^{(\bar{\nu},\nu)}(\nu,q^2)=\frac{1}{\pi}\operatorname{Im}T_i^{(\bar{\nu},\nu)}(s,0,q^2,q^2)\qquad(i=1,2,3). \tag{2.41}$$

III. CROSSING AND ISOSPIN PROPERTIES

Because the amplitude A_{ij}, defined in (2.29), is a Lorentz invariant, it has the simple transformation properties of a spinless amplitude under crossing. In the following we investigate the consequences of the constraints of crossing and isospin invariance on A_{ij}.

Assuming that isospin is conserved, the amplitude A_{ij} may be decomposed into amplitudes of definite isospin I, denoted by A^I_{ij}. Now A^I_{ij}, in general, receives contributions from resonances and nondiffractive Regge exchanges, as well as from the Pomeron, which is responsible for diffractive scattering. Therefore, we shall assume[10] that

$$A^I_{ij}(s,t,q_1^2,q_2^2)=F^I_{ij}(s,t,q_1^2,q_2^2)+P^I_{ij}(s,t,q_1^2,q_2^2), \tag{3.1}$$

where F is the nondiffractive contribution and P is the Pomeron contribution.

First, consider $i=j=3$. Our treatment is similar to that in Ref. 11. We have

$$A_{33}(s,t,q_1^2,q_2^2)=\tfrac{1}{3}A^{1/2}_{33}(s,t,q_1^2,q_2^2)+\tfrac{2}{3}A^{3/2}_{33}(s,t,q_1^2,q_2^2), \tag{3.2}$$

and

$$\begin{aligned}A^{\bar\nu}_V(s,t,q_1^2,q_2^2)&=\tfrac{4}{3}A^{1/2}_{33}(s,t,q_1^2,q_2^2)+\tfrac{2}{3}A^{3/2}_{33}(s,t,q_1^2,q_2^2),\\ A^{\nu}_V(s,t,q_1^2,q_2^2)&=2A^{3/2}_{33}(s,t,q_1^2,q_2^2).\end{aligned} \tag{3.3}$$

We shall suppress q_1^2 and q_2^2 whenever there is no danger of confusion. The nondiffractive amplitude $F^{1/2}_{33}$ is assumed to have resonances lying on the nucleon trajectory in the s channel and t channel resonances on the exchange-degenerate ρ-P'-A_2 trajectory. Similarly, $F^{3/2}_{33}$ has s channel resonances on the Δ trajectory and t channel resonances on the ρ-P'-A_2 trajectory. The diffractive parts, $P^{1/2}_{33}$ and $P^{3/2}_{33}$, have a Pomeron exchanged in the t channel and no s channel resonances.

With these assumptions, our amplitude $F^{3/2}_{33}$ may be written as

$$F^{3/2}_{33}(s,t,u)=aF^{33}_{\Delta}(s,t)+bF^{33}_{\Delta}(u,t)+cF^{33}_{N}(u,t), \tag{3.4}$$

where it is assumed that $F_\Delta(s,t)$ has s channel resonances lying on the Δ trajectory and that $F_N(s,t)$ has s channel resonances on the nucleon trajectory.

In order to determine a, b, and c and to construct the $I=\frac{1}{2}$ amplitude, we use the isospin s-u crossing relations and crossing symmetry, which give

$$A^{1/2}_{33}(s,t,u)=-\tfrac{1}{2}A^{3/2}_{33}(s,t,u)+\tfrac{3}{2}A^{3/2}_{33}(u,t,s). \tag{3.5}$$

From (3.4) and (3.5), we have

$$\begin{aligned}F^{1/2}_{33}(s,t,u)=&-\tfrac{1}{2}[aF^{33}_{\Delta}(s,t)+bF^{33}_{\Delta}(u,t)+cF^{33}_{N}(u,t)]\\&+\tfrac{3}{2}[aF^{33}_{\Delta}(u,t)+bF^{33}_{\Delta}(s,t)+cF^{33}_{N}(s,t)].\end{aligned} \tag{3.6}$$

The coefficient of $F^{33}_{\Delta}(s,t)$ in (3.6) must be zero. Then, by absorbing the constants a and $\frac{3}{2}c$ in $F^{33}_{\Delta}(s,t)$ and $F^{33}_{N}(s,t)$, respectively, we obtain

$$\begin{aligned}F^{3/2}_{33}(s,t,u)&=F^{33}_{\Delta}(s,t)+\tfrac{1}{3}F^{33}_{\Delta}(u,t)+\tfrac{2}{3}F^{33}_{N}(u,t),\\ F^{1/2}_{33}(s,t,u)&=F^{33}_{N}(s,t)-\tfrac{1}{3}F^{33}_{N}(u,t)+\tfrac{4}{3}F^{33}_{\Delta}(u,t).\end{aligned} \tag{3.7}$$

The construction of the Pomeron part follows the discussion of Ref. 11. We have

$$P^{1/2}_{33}(s,t,u)=P^{3/2}_{33}(s,t,u)=A^{33}_P(t,s)+A^{33}_P(t,u). \tag{3.8}$$

For the case where $i=j=8$, we find that

$$\begin{aligned}F^{1/2}_{88}(s,t,u)&=F^{88}_{N}(s,t)+F^{88}_{N}(u,t),\\ P^{1/2}_{88}(s,t,u)&=A^{88}_P(t,s)+A^{88}_P(t,u).\end{aligned} \tag{3.9}$$

For $i=3$, $j=8$, we get

$$F^{1/2}_{38}(s,t,u)=F^{38}_{N}(s,t)+F^{38}_{N}(u,t). \tag{3.10}$$

In the latter case, the t channel has $I=1$, so there is no Pomeron, and the term contributes with opposite sign to proton and neutron scattering. Time reversal, given by Eq. (2.16), implies that

$$F^{1/2}_{83}(s,t,q_1^2,q_2^2)=F^{1/2}_{38}(s,t,q_2^2,q_1^2). \tag{3.11}$$

With the help of (3.2) and (3.3), the Compton and neutrino amplitudes for scattering off protons become, using (2.19),

$$\begin{aligned}A_{33}(s,t,q_1^2,q_2^2)=&A^{33}_P(t,s,q_1^2,q_2^2)\\&+\tfrac{1}{3}A^{88}_P(t,s,q_1^2,q_2^2)\\&+\tfrac{1}{3}F^{33}_N(s,t,q_1^2,q_2^2)\\&+\tfrac{2}{3}F^{33}_\Delta(s,t,q_1^2,q_2^2)\\&+\tfrac{1}{3}F^{88}_N(s,t,q_1^2,q_2^2)\\&+\frac{1}{\sqrt{3}}[F^{38}_N(s,t,q_1^2,q_2^2)\\&+F^{38}_N(s,t,q_2^2,q_1^2)]\\&+(s\rightarrow u),\end{aligned} \tag{3.12}$$

$$A^{\bar\nu}_V(s,t)=2A^{33}_P(t,s)+2A^{33}_P(t,u)+\tfrac{4}{3}F^{33}_N(s,t)+\tfrac{2}{3}F^{33}_\Delta(s,t)+2F^{33}_\Delta(u,t), \tag{3.13}$$

and

$$A^{\nu}_V(s,t)=2A^{33}_P(t,s)+2A^{33}_P(t,u)+2F^{33}_\Delta(s,t)+\tfrac{2}{3}F^{33}_\Delta(u,t)+\tfrac{4}{3}F^{33}_N(u,t). \tag{3.14}$$

The neutron Compton amplitude is given by (3.12), with the sign of F^{38}_N reversed.

IV. MODELS FOR THE AMPLITUDES

The following models for the Pomeron and Regge amplitudes are based on the analytic model of Refs. 10 and 11. Let us consider A_P^{33}, which is given by

$$A_P^{33}(t, s, q_1^2, q_2^2) = \gamma_P^{33}(t) \ln[1 + (1-\omega')^{1/2}] \times w_P(\omega')^{\alpha_P(t)-2} \mathfrak{F}(q_1^2, q_2^2) \times D_3(q_1^2) D_3(q_2^2). \quad (4.1)$$

The variable ω' is defined by

$$\omega' = 1 + x_1 x_2 (s - s_t), \quad (4.2)$$

where

$$x_i = [a + (q_t^2 - q_i^2)^{1/2}]^{-1} \quad (i = 1, 2), \quad (4.3)$$

s_t is the inelastic s-channel threshold,

$$s_t = (M + m_\pi)^2, \quad (4.4)$$

q_t is a constant, and a is a positive constant. The function x_1 has a cut on the real q_1^2 axis in the region $q_t^2 \leq q_1^2 \leq \infty$, and similarly for x_2. We note that for $q_1^2 = q_2^2 = q^2$,

$$\lim_{\substack{|q^2| \to \infty \\ s \to \infty}} \omega' = \omega, \quad (4.5)$$

where ω is the usual scaling variable

$$\omega = 1 + \frac{s - M^2}{-q^2}. \quad (4.6)$$

The function $(1-\omega')^{1/2}$ is defined by

$$(1-\omega')^{1/2} \equiv (x_1)^{1/2} (x_2)^{1/2} (s_t - s)^{1/2}. \quad (4.7)$$

The residue γ_P^{33}, propagator D_3, etc., are discussed in detail later in this section.

For A_P^{88} we take a function which differs from (4.1) only in its residue function and q^2 dependence:

$$A_P^{88}(t, s, q_1^2, q_2^2) = \gamma_P^{88}(t) \ln[1 + (1-\omega')^{1/2}] w_P(\omega')^{\alpha_P(t)-2} \mathfrak{F}(q_1^2, q_2^2) D_8(q_1^2) D_8(q_2^2). \quad (4.8)$$

For the nondiffractive part, we have

$$F_N^{33}(s, t, q_1^2, q_2^2) = -[\gamma_N^{33}(s) \Gamma(\tfrac{3}{2} - \alpha_N(s)) w_\rho(t)^{\alpha_N(s)} + \gamma_{1\rho}^{33}(t) \Gamma(2 - \alpha_\rho(t)) w_N^{33}(\omega')^{\alpha_\rho(t)-2}] \mathfrak{F}(q_1^2, q_2^2) D_3(q_1^2) D_3(q_2^2) + \sum(\text{satellites}). \quad (4.9)$$

Here, provision has been made for satellites.

Our function F_Δ^{33} is similar to F_N^{33}:

$$F_\Delta^{33}(s, t, q_1^2, q_2^2) = -[\gamma_\Delta^{33}(s) \Gamma(\tfrac{3}{2} - \alpha_\Delta(s)) w_\rho(t)^{\alpha_\Delta(s)} + \gamma_{2\rho}^{33}(t) \Gamma(2 - \alpha_\rho(t)) w_\Delta^{33}(\omega')^{\alpha_\rho(t)-2}] \mathfrak{F}(q_1^2, q_2^2) D_3(q_1^2) D_3(q_2^2) + \sum(\text{satellites}). \quad (4.10)$$

The nondiffractive contribution to the scattering of isoscalar photons is given by

$$F_N^{88}(s, t, q_1^2, q_2^2) = -[\gamma_N^{88}(s) \Gamma(\tfrac{3}{2} - \alpha_N(s)) w_\rho(t)^{\alpha_N(s)} + \gamma_\rho^{88}(t) \Gamma(2 - \alpha_\rho(t)) w_N^{88}(\omega')^{\alpha_\rho(t)-2}] \mathfrak{F}(q_1^2, q_2^2) D_8(q_1^2) D_8(q_2^2) + \sum(\text{satellites}). \quad (4.11)$$

Finally, the A_2(isoscalar-isovector) contribution is

$$F_N^{38}(s, t, q_1^2, q_2^2) = -[\gamma_N^{38}(s) \Gamma(\tfrac{3}{2} - \alpha_N(s)) w_\rho(t)^{\alpha_N(s)} + \gamma_{1\rho}^{38}(t) \Gamma(2 - \alpha_\rho(t)) w_{1N}^{38}(\omega')^{\alpha_\rho(t)-2} + \gamma_{2\rho}^{38}(t) \Gamma(2 - \alpha_\rho(t)) w_{2N}^{38}(\omega')^{\alpha_\rho(t)-3}] \mathfrak{F}(q_1^2, q_2^2) D_3(q_1^2) D_8(q_2^2) + \sum(\text{satellites}). \quad (4.12)$$

Here we have explicitly included a satellite for the A_2.

We list the residues, trajectories, etc., and examine some of their properties.

(1) Residues. The Pomeron residue $\gamma_P^{33}(t)$ is a suitable real analytic function (with possible unitarity cuts and poles on the second sheet). We require that $\gamma_P^{33}(t) \to 0$ as $t \to \pm\infty$. For small $|t|$, $\gamma_P^{33}(t)$ has the approximate form

$$\gamma_P^{33}(t) \simeq e^{g_P(\alpha_P(t)-1)} \gamma_P^{33} / \Gamma(\alpha_P(t)). \quad (4.13)$$

The residue $\gamma_P^{88}(t)$ is similar, with γ_P^{33} replaced by γ_P^{88}. For $\gamma_{1\rho}^{33}(t)$, we take

$$\gamma_{1\rho}^{33}(t) = \frac{\gamma_{1\rho}^{33} e^{g_{P'}(\alpha_\rho(t)-1/2)}}{[1 + (4M^2 - t)^{1/2}/\Lambda_\rho]^{q_\rho}}, \quad (4.14)$$

where in (4.13) and (4.14) g_P, $g_{P'}$, Λ_ρ, and q_ρ are constants. The residue function is real analytic, has poles only on the second sheet, and possesses the elastic unitarity cut. The constant Λ_ρ is chosen large, so that, for t near threshold (4.14) may be approximated by its numerator. The residues

$\gamma_{2\rho}^{33}(t)$, $\gamma_{\rho}^{88}(t)$, $\gamma_{1\rho}^{38}(t)$, and $\gamma_{2\rho}^{38}(t)$ are similar, with $\gamma_{1\rho}^{33}$ replaced by $\gamma_{2\rho}^{33}$, γ_{ρ}^{88}, $\gamma_{1\rho}^{38}$, and $\gamma_{2\rho}^{38}$, respectively. For $\gamma_{1\rho}^{38}(t)$ and $\gamma_{2\rho}^{38}(t)$, we also replace $g_{P'}$ by g_{A_2}.

The direct-channel residue is given by

$$\gamma_N^{33}(s)=\frac{\gamma_N^{33}}{[1+(s_t-s)^{1/2}/\Lambda_N]^{2a_N}}\,. \tag{4.15}$$

This is a real analytic function, has poles only on the second sheet, and has the inelastic unitarity cut. We have

$$\gamma_N^{33}(s)\to 0 \text{ as } s\to\pm\infty\,. \tag{4.16}$$

Again, Λ_N is chosen large so that $\gamma_N^{33}(s)\simeq\gamma_N^{33}$ for s near threshold. The residues $\gamma_{\Delta}^{33}(s)$, $\gamma_N^{88}(s)$, and $\gamma_N^{38}(s)$ are similar in form to $\gamma_N^{33}(s)$, and have the property analogous to (4.16).

(2) w functions. For the Pomeron we take

$$w_P(\omega')=A_P+B_P\omega'+C_P(1-\omega')^{1/2}\,. \tag{4.17}$$

Because of (4.7), the function $w_P(\omega')$ has a cut in s beginning at the inelastic threshold. The constants A_P, B_P, and C_P satisfy the following conditions:

$$\begin{aligned}&A_P>0\,,\quad B_P<0\,,\quad C_P>0\,,\\&0\le C_P{}^2+4B_P(A_P+B_P)\le C_P{}^2\,.\end{aligned} \tag{4.18}$$

The conditions (4.18) ensure that $w_P(\omega')^{\alpha_P(t)-2}$ is analytic in s for fixed $q_1{}^2$ and $q_2{}^2$.

Proof. Let $z=(s_t-s)^{1/2}$. Cuts are generated when $w_P(\omega')=0$. This has the solution

$$z=\frac{-C_P\pm[C_P{}^2+4B_P(A_P+B_P)]^{1/2}}{-2B_P(x_1)^{1/2}(x_2)^{1/2}}\,.$$

For the choice of conditions on A_P, B_P, and C_P described above, and in the physical $q_1{}^2$ and $q_2{}^2$ sheets, we have $\mathrm{Re}\,z<0$, so the cuts occur only in the second sheet of the s plane. Similarly, the function $\ln[1+(1-\omega')^{1/2}]$ is analytic in the first sheet. It can be shown that $w_P(\omega')^{\alpha_P(t)-2}$ and $\ln[1+(1-\omega')^{1/2}]$ are analytic in $q_1{}^2$ and $q_2{}^2$, separately, for $s>s_t$, but that for $s<s_t$, cuts appear in the physical $q_1{}^2$ and $q_2{}^2$ sheets. However, when $q_1{}^2=q_2{}^2=q^2$, then they are analytic in q^2 for all values of s.

For the remaining w functions, we take

$$\begin{aligned}&w_N^{33}(\omega')=A_N+B_N\omega'+C_N(1-\omega')^{1/2}\,,\\&w_{\Delta}^{33}(\omega')=w_N^{88}(\omega')=w_N^{33}(\omega')\,,\\&w_{1N}^{38}(\omega')=A_{1N}+B_{1N}\omega'+C_{1N}(1-\omega')^{1/2}\,,\\&w_{2N}^{38}(\omega')=A_{2N}+B_{2N}\omega'+C_{2N}(1-\omega')^{1/2}\,,\end{aligned} \tag{4.19}$$

and

$$w_{\rho}(t)=A_{\rho}+B_{\rho}t+C_{\rho}[(2M+m_{\pi})^2-t]^{1/2}\,. \tag{4.20}$$

Constraints analogous to those in (4.18) hold here:

$$\begin{aligned}&A_i>0\,,\quad B_i<0\,,\quad C_i>0\,,\qquad (i=N,\,1N,\,2N,\,\rho)\\&0\le C_i{}^2+4B_i(A_i+B_i)\le C_i{}^2\,.\end{aligned} \tag{4.21}$$

(3) Trajectories. Our Pomeron trajectory is given by

$$\alpha_P(t)=1+b_Pt\left[1+\left(\frac{(2M+m_{\pi})^2-t}{\Delta_P}\right)^{1/2}\right]^{-2}. \tag{4.22}$$

This has a cut beginning at the t-channel inelastic threshold, and satisfies

$$\alpha_P(\pm\infty)=1-b_P\Delta_P\,. \tag{4.23}$$

The exchange-degenerate ρ-P'-A_2 trajectory α_{ρ}, and the nucleon and Δ trajectories, α_N and α_{Δ}, are given by

$$\alpha_{\rho}(t)=a_{\rho}+\frac{b_{\rho}t-c_{\rho}(4M^2-t)^{1/2}}{\{1+[(4M^2-t)/\Delta_{\rho}]^{1/2}\}^2}\,, \tag{4.24}$$

$$\alpha_N(s)=a_N+\frac{b_Ns-c_N(s_t-s)^{1/2}}{\{1+[(s_t-s)/\Delta_N]^{1/2}\}^2}\,, \tag{4.25}$$

and

$$\alpha_{\Delta}(s)=a_{\Delta}+\frac{b_{\Delta}s-c_{\Delta}(s_t-s)^{1/2}}{\{1+[(s_t-s)/\Delta_{\Delta}]^{1/2}\}^2}\,. \tag{4.26}$$

These trajectories are real analytic, and have poles only in the second sheet. The ρ trajectory has the elastic unitarity cut, while α_N and α_{Δ} have the inelastic cut. In the asymptotic region $\alpha_N(\pm\infty)$ is given by

$$\alpha_N(\pm\infty)=a_N-b_N\Delta_N\simeq -b_N\Delta_N\,, \tag{4.27}$$

and similarly for α_{Δ}. In what follows, we shall assume that $\alpha_P(0)=1$ and that $\alpha_{\rho}(0)=\frac{1}{2}$.

(4) Propagators. Vector dominance in our model is manifested by the appearance of the isovector and isoscalar propagators D_3 and D_8, respectively. The propagator D_3 represents the contribution of a vector meson, which we take to be the ρ, to isovector photon scattering. Our model, which is based on a ρ-dominance model for the nucleon form factor,[17] is given by

$$D_3(q^2)=[q^2-m_{\rho}{}^2-\Gamma_3(4m_{\pi}{}^2-q^2)^{1/2}]^{-1}\,, \tag{4.28}$$

where

$$\Gamma_3=\frac{m_{\rho}\Gamma_{\rho}}{(m_{\rho}{}^2-4m_{\pi}{}^2)^{1/2}}\,. \tag{4.29}$$

For the isoscalar propagator, we have

$$D_8(q^2)=[q^2-m_{\omega}{}^2-\Gamma_8(9m_{\pi}{}^2-q^2)^{1/2}]^{-1}\,, \tag{4.30}$$

where

$$\Gamma_8=\frac{m_{\omega}\Gamma_{\omega}}{(m_{\omega}{}^2-9m_{\pi}{}^2)^{1/2}}\,. \tag{4.31}$$

We have chosen the ω to dominate isoscalar photon scattering, and have therefore neglected the contribution of the ϕ meson and other intermediate states. This simplifies our model considerably, and also allows us to predict photoproduction and electroproduction of ρ and ω mesons in Sec. VI. The propagators D_3 and D_8 have poles only on the second sheet in q^2.

Our q^2-dependent function $\mathfrak{F}$ is given by

$$\mathfrak{F}(q_1^2, q_2^2) = 1 + f(q_1^2) f(q_2^2), \tag{4.32}$$

where

$$f(q^2) = \frac{c q^2 (m_\omega^2 - q^2)}{[a + (q_t^2 - q^2)^{1/2}]^n}. \tag{4.33}$$

The constants a and q_t are the same as in (4.3) and c is a parameter. We will assume that the power $n > 4$, so that

$$\lim_{|q^2| \to \infty} \mathfrak{F}(q^2, q^2) = 1. \tag{4.34}$$

The function $\mathfrak{F}(q_1^2, q_2^2)$ is analytic in q_1^2 and q_2^2, with cuts in the region $q_t^2 \leq q_i^2 \leq \infty$ $(i = 1, 2)$.

We are now in a position to enumerate the properties of our Compton amplitude (3.12).

(i) It has poles in q_1^2 and q_2^2 at the vector-meson masses, arising from $D_3(q^2)$ and $D_8(q^2)$. The poles lie in the second sheet and provide for the correct ρ and ω widths.

(ii) Resonances in the t channel and s channel are manifested as poles in t for $\alpha_\rho(t) = 2, 3, 4, \ldots$, and poles in s for $\alpha_N(s) = \frac{3}{2}, \frac{5}{2}, \ldots$, and for $\alpha_\Delta(s) = \frac{3}{2}, \frac{5}{2}, \ldots$. As discussed in item (3) above, the poles lie in the second sheet. The Born term (nucleon pole) is added separately, as in the discussion following (2.29) of Sec. II.

(iii) For large s at fixed t, there is Regge asymptotic behavior. For instance, provided that $q_N = b_\rho \Delta_\rho$, we have

$$F_N^{33}(s, t, q_1^2, q_2^2) + F_N^{33}(u, t, q_1^2, q_2^2) \simeq \frac{\pi \gamma_{1\rho}^{33}(t)}{\Gamma(\alpha_\rho(t) - 1)} \left(\frac{s}{s_0}\right)^{\alpha_\rho(t) - 2} \left(\frac{1 + e^{-i\pi\alpha_\rho(t)}}{\sin \pi \alpha_\rho(t)}\right) \times \mathfrak{F}(q_1^2, q_2^2) D_3(q_1^2) D_3(q_2^2), \tag{4.35}$$

where

$$s_0 = (|B_N| x_1 x_2)^{-1}. \tag{4.36}$$

The combination (4.35) appears in the Compton amplitude, and has the correct signature factor. The result for the Pomeron amplitude is

$$A_P^{33}(t, s, q_1^2, q_2^2) + A_P^{33}(t, u, q_1^2, q_2^2) \simeq \frac{\gamma_P^{33}(t)}{2} \left(\frac{s}{s_{0P}}\right)^{\alpha_P(t) - 2} \left[\ln\left(\frac{s}{|B_P| s_{0P}}\right)(1 + e^{-i\pi\alpha_P(t)}) - i\pi e^{-i\pi\alpha_P(t)}\right] \mathfrak{F}(q_1^2, q_2^2) D_3(q_1^2) D_3(q_2^2), \tag{4.37}$$

where $s_{0P} = (|B_P| x_1 x_2)^{-1}$.

(iv) The model possesses Regge behavior at fixed s for large t. If $q_\rho = b_N \Delta_N$, then in the Regge limit

$$F_N^{33}(s, t, q_1^2, q_2^2) \simeq \frac{-\pi \gamma_N^{33}(s)(-t/t_0)^{\alpha_N(s)}}{\Gamma(\alpha_N(s) - \frac{1}{2}) \sin \pi(\alpha_N(s) - \frac{1}{2})} \times \mathfrak{F}(q_1^2, q_2^2) D_3(q_1^2) D_3(q_2^2), \tag{4.38}$$

where $t_0 = 1/|B_\rho|$.

(v) The amplitude A_{33}, defined in (3.12), is $s \leftrightarrow u$ crossing symmetric.

(vi) It was assumed in Sec. II that the amplitudes (3.12), (3.13), and (3.14) satisfy a Mandelstam representation. By employing the discussion in item (2) above, it is easy to show that our model satisfies this requirement provided that $q_1^2 < q_t^2$ and $q_2^2 < q_t^2$. However, if for instance $q_1^2 > q_t^2$, then the function $(1 - \omega')^{1/2}$ is not a real analytic function of s, and, as a result, our model amplitudes are not Mandelstam analytic. The model is also analytic in q^2 for all values of s, t, and u.

Let us discuss the application of our model to various physical processes.

A. Structure Functions

The structure functions for electroproduction and neutrino scattering are defined in (2.35) and (2.41), respectively. For $T_2(s, t, q^2, q^2)$, the discontinuity across the positive s axis $\Delta_s T_2(s, t, q^2, q^2)$ is given by

$$\Delta_s T_2(s, t, q^2, q^2) = \frac{1}{2i} \lim_{\epsilon \to 0} [T_2(s + i\epsilon, t, q^2, q^2) - T_2(s - i\epsilon, t, q^2, q^2)]. \tag{4.39}$$

For $q^2 < q_t^2$, we have

$$w_P(\omega' \pm i\epsilon) = A_P + B_P \omega' \mp i C_P (\omega' - 1)^{1/2} = |w_P(\omega')| e^{\mp i \phi_P(\omega')}, \tag{4.40}$$

where

$$\phi_P(\omega') = \tan^{-1}\left(\frac{C_P(\omega' - 1)^{1/2}}{A_P + B_P \omega'}\right). \tag{4.41}$$

Therefore, upon taking the absorptive part in

(3.12), we obtain the electroproduction structure function

$$\nu W_2(\nu, q^2) = \nu W_2^P(\nu, q^2) + \nu W_2^{P'}(\nu, q^2) + \nu W_2^{A_2}(\nu, q^2) + \nu W_2^{A_2'}(\nu, q^2) + (\text{Born term}) + (\text{resonances}) + \sum(\text{satellites}), \tag{4.42}$$

where

$$\nu W_2^P(\nu, q^2) = -\frac{q^2\nu}{\pi}\mathfrak{F}(q^2, q^2)\left[\gamma_P^{33}[D_3(q^2)]^2 + \tfrac{1}{3}\gamma_P^{88}[D_8(q^2)]^2\right] \times \left\{\tfrac{1}{2}\ln(\omega')\sin(\phi_P(\omega')) - \tan^{-1}[(\omega'-1)^{1/2}]\cos(\phi_P(\omega'))\right\}|w_P(\omega')|^{-1}, \tag{4.43}$$

$$\nu W_2^{P'}(\nu, q^2) = \frac{q^2\nu\Gamma(3/2)}{3\pi}\mathfrak{F}(q^2, q^2)\left[(\gamma_{1\rho}^{33} + 2\gamma_{2\rho}^{33})[D_3(q^2)]^2 + \gamma_\rho^{88}[D_8(q^2)]^2\right]\sin(\tfrac{3}{2}\phi_N^{33}(\omega'))|w_N^{33}(\omega')|^{-3/2}, \tag{4.44}$$

$$\nu W_2^{A_2}(\nu, q^2) = \frac{2q^2\nu\Gamma(3/2)}{\sqrt{3}\,\pi}\mathfrak{F}(q^2, q^2)\gamma_{1\rho}^{38} D_3(q^2) D_8(q^2)\sin(\tfrac{3}{2}\phi_{1N}^{38}(\omega'))|w_{1N}^{38}(\omega')|^{-3/2}, \tag{4.45}$$

$$\nu W_2^{A_2'}(\nu, q^2) = \frac{2q^2\nu\Gamma(3/2)}{\sqrt{3}\,\pi}\mathfrak{F}(q^2, q^2)\gamma_{2\rho}^{38} D_3(q^2) D_8(q^2)\sin(\tfrac{5}{2}\phi_{2N}^{38}(\omega'))|w_{2N}^{38}(\omega')|^{-5/2}. \tag{4.46}$$

Here $\phi_N^{33}(\omega')$, $\phi_{1N}^{38}(\omega')$, and $\phi_{2N}^{38}(\omega')$ are the equivalents of (4.41) for the Regge terms.

We expect νW_2 to be scale-invariant in the Bjorken limit $-q^2 \to \infty$, ω fixed. For any fixed ω, $s \to \infty$ and because of the property (4.16) of the residues, the direct-channel resonance terms, as well as the Born term, vanish in the Bjorken limit. Furthermore, by (4.5) the variable ω' reduces to the scaling variable ω. Upon taking the limit in (4.42) and neglecting satellite terms, the scale-invariant result is found to be

$$\nu W_2(\nu, q^2) \xrightarrow[-q^2\to\infty]{} F_2(\omega) = F_2^P(\omega) + F_2^{P'}(\omega) + F_2^{A_2}(\omega) + F_2^{A_2'}(\omega), \tag{4.47}$$

where

$$F_2^P(\omega) = \gamma_P\omega\left\{\tfrac{1}{2}\ln(\omega)\sin\phi_P(\omega) - \tan^{-1}[(\omega-1)^{1/2}]\cos\phi_P(\omega)\right\} \times |w_P(\omega)|^{-1}, \tag{4.48}$$

$$F_2^{P'}(\omega) = -\gamma_{P'}\omega\sin(\tfrac{3}{2}\phi_N^{33}(\omega))|w_N^{33}(\omega)|^{-3/2}, \tag{4.49}$$

$$F_2^{A_2}(\omega) = -\gamma_{A_2}\omega\sin(\tfrac{3}{2}\phi_{1N}^{38}(\omega))|w_{1N}^{38}(\omega)|^{-3/2}, \tag{4.50}$$

$$F_2^{A_2'}(\omega) = -\gamma_{A_2'}\omega\sin(\tfrac{5}{2}\phi_{2N}^{38}(\omega))|w_{2N}^{38}(\omega)|^{-5/2}. \tag{4.51}$$

Here, we have made the definitions

$$\gamma_P = \frac{\gamma_P^{33} + \frac{1}{3}\gamma_P^{88}}{2\pi M}, \quad \gamma_{P'} = \frac{\Gamma(\frac{3}{2})}{2\pi M}(\tfrac{1}{3}\gamma_{1\rho}^{33} + \tfrac{2}{3}\gamma_{2\rho}^{33} + \tfrac{1}{3}\gamma_\rho^{88}), \quad \gamma_{A_2} = \frac{\Gamma(\frac{3}{2})}{\sqrt{3}\,\pi M}\gamma_{1\rho}^{38}, \quad \gamma_{A_2'} = \frac{\Gamma(\frac{3}{2})}{\sqrt{3}\,\pi M}\gamma_{2\rho}^{38}, \tag{4.52}$$

By using (3.13) and (3.14), we easily obtain the sum of the scale-invariant neutrino and antineutrino structure functions

$$F_{2V}^{\bar{\nu}p}(\omega) + F_{2V}^{\nu p}(\omega) = \frac{2\omega}{\pi M}\gamma_P^{33}\left\{\tfrac{1}{2}\ln(\omega)\sin\phi_P(\omega) - \tan^{-1}[(\omega-1)^{1/2}]\cos\phi_P(\omega)\right\}|w_P(\omega)|^{-1} - \frac{2\Gamma(\frac{3}{2})}{3\pi M}(\gamma_{1\rho}^{33} + 2\gamma_{2\rho}^{33})\omega\sin(\tfrac{3}{2}\phi_N^{33}(\omega))|w_N^{33}(\omega)|^{-3/2}. \tag{4.53}$$

B. Compton Scattering

Using (2.39), we obtain the following result for the total photoabsorption cross section:

$$\sigma(\gamma p) = \sigma_P + \sigma_{P'} + \sigma_{A_2} + \sigma_{A_2'} + (\text{Born term}) + (\text{resonances}) + \sum(\text{satellites}), \tag{4.54}$$

where

$$\sigma_P = 4\pi\alpha\nu\gamma_{Pc}\left\{\tfrac{1}{2}\ln(\omega')\sin\phi_P(\omega') - \tan^{-1}[(\omega'-1)^{1/2}]\cos\phi_P(\omega')\right\} \times |w_P(\omega')|^{-1}, \tag{4.55}$$

$$\sigma_{P'} = -4\pi\alpha\nu\gamma_{P'c}\sin(\tfrac{3}{2}\phi_N^{33}(\omega'))|w_N^{33}(\omega')|^{-3/2}, \tag{4.56}$$

$$\sigma_{A_2} = -\frac{8\pi\Gamma(\frac{3}{2})\alpha\nu}{\sqrt{3}}\gamma_{1\rho}^{38}D_3(0)D_8(0)\sin(\tfrac{3}{2}\phi_{1N}^{38}(\omega'))\times|w_{1N}^{38}(\omega')|^{-3/2}, \tag{4.57}$$

$$\sigma_{A_2'} = -\frac{8\pi\Gamma(\frac{3}{2})\alpha\nu}{\sqrt{3}}\gamma_{2\rho}^{38}D_3(0)D_8(0)\sin(\tfrac{5}{2}\phi_{2N}^{38}(\omega'))\times|w_{2N}^{38}(\omega')|^{-5/2}. \tag{4.58}$$

Here, the Compton residues are defined by

$$\gamma_{Pc} = \gamma_P^{33}[D_3(0)]^2 + \tfrac{1}{3}\gamma_P^{88}[D_8(0)]^2, \tag{4.59}$$

$$\gamma_{P'c} = \Gamma(\tfrac{3}{2})\{(\tfrac{1}{3}\gamma_{1\rho}^{33} + \tfrac{2}{3}\gamma_{2\rho}^{33})[D_3(0)]^2 + \tfrac{1}{3}\gamma_\rho^{88}[D_8(0)]^2\}.$$

The differential Compton cross section is given by (2.34). If we neglect the direct channel resonance terms, our model for T_2 reads

$$\begin{aligned}T_2(s,t,0,0) = -(q_1\cdot q_2)\Big\{&(\gamma_P^{33}(t)[D_3(0)]^2 + \tfrac{1}{3}\gamma_P^{88}(t)[D_8(0)]^2)\ln[1+(1-\omega')^{1/2}]w_P(\omega')^{\alpha_P(t)-2}\\ &-[(\tfrac{1}{3}\gamma_{1\rho}^{33}(t)+\tfrac{2}{3}\gamma_{2\rho}^{33}(t))[D_3(0)]^2 + \tfrac{1}{3}\gamma_\rho^{88}(t)[D_8(0)]^2]\Gamma(2-\alpha_\rho(t))w_N^{33}(\omega')^{\alpha_\rho(t)-2}\\ &-\frac{2}{\sqrt{3}}\gamma_{1\rho}^{38}(t)D_3(0)D_8(0)\Gamma(2-\alpha_\rho(t))w_{1N}^{38}(\omega')^{\alpha_\rho(t)-2}\\ &-\frac{2}{\sqrt{3}}\gamma_{2\rho}^{38}(t)D_3(0)D_8(0)\Gamma(2-\alpha_\rho(t))w_{2N}^{38}(\omega')^{\alpha_\rho(t)-3}\Big\} + (s\leftrightarrow u).\end{aligned} \tag{4.60}$$

The neglect of resonances should not be too important at high energy, where the Regge terms dominate.

C. Vector-Meson Photoproduction and Electroproduction

Because of our vector dominance assumption, we may treat vector-meson photoproduction and electroproduction by taking the residue at the pole $q_2^2 = m_V^2$ in (3.12). If we denote the Compton amplitude by $T_2(\gamma\gamma)$ and the ρ photoproduction amplitude by $T_2(\gamma\rho)$, this means that

$$T_2(\gamma\rho) = \lim_{\substack{q_1^2\to 0\\ q_2^2\to m_\rho^2}}\frac{1}{D_3(q_2^2)}\left(\frac{f_\rho}{e m_\rho^2}\right)T_2(\gamma\gamma), \tag{4.61}$$

where f_ρ is the ρ-meson–photon coupling constant. By the limit as $q_2^2 \to m_\rho^2$, we mean that one should go to the pole in D_3, although m_ρ^2 is taken real in $T_2(\gamma\gamma)$. Thus those amplitudes which do not contain $D_3(q_2^2)$ vanish in the limit, and we obtain

$$\begin{aligned}T_2(\gamma\rho) = -\frac{(q_1\cdot q_2)}{e m_\rho^2}f_\rho\Big[&\gamma_P^{33}(t)D_3(0)\ln[1+(1-\omega')^{1/2}]w_P(\omega')^{\alpha_P(t)-2}\\ &-(\tfrac{1}{3}\gamma_{1\rho}^{33}(t)+\tfrac{2}{3}\gamma_{2\rho}^{33}(t))D_3(0)\Gamma(2-\alpha_\rho(t))w_N^{33}(\omega')^{\alpha_\rho(t)-2}\\ &-\frac{1}{\sqrt{3}}\gamma_{1\rho}^{38}(t)D_8(0)\Gamma(2-\alpha_\rho(t))w_{1N}^{38}(\omega')^{\alpha_\rho(t)-2}\\ &-\frac{1}{\sqrt{3}}\gamma_{2\rho}^{38}(t)D_8(0)\Gamma(2-\alpha_\rho(t))w_{2N}^{38}(\omega')^{\alpha_\rho(t)-3}\Big] + (s\leftrightarrow u),\end{aligned} \tag{4.62}$$

where we have neglected the resonances. Similar arguments furnish the ω photoproduction amplitude:

$$\begin{aligned}T_2(\gamma\omega) = -\frac{(q_1\cdot q_2)}{e m_\omega^2}f_\omega\Big[&\tfrac{1}{3}\gamma_P^{88}(t)D_8(0)\ln[1+(1-\omega')^{1/2}]w_P(\omega')^{\alpha_P(t)-2}\\ &-\tfrac{1}{3}\gamma_\rho^{88}(t)D_8(0)\Gamma(2-\alpha_\rho(t))w_N^{33}(\omega')^{\alpha_\rho(t)-2}\\ &-\frac{1}{\sqrt{3}}\gamma_{1\rho}^{38}(t)D_3(0)\Gamma(2-\alpha_\rho(t))w_{1N}^{38}(\omega')^{\alpha_\rho(t)-2}\\ &-\frac{1}{\sqrt{3}}\gamma_{2\rho}^{38}(t)D_3(0)\Gamma(2-\alpha_\rho(t))w_{2N}^{38}(\omega')^{\alpha_\rho(t)-3}\Big] + (s\leftrightarrow u).\end{aligned} \tag{4.63}$$

The differential cross section for vector-meson photoproduction is obtained by substituting (4.62) or (4.63) for T_2 in (2.34).

The cross section for production of vector mesons by means of virtual photons may be separated out from the cross section for electroproduction of vector mesons,[18] $e+p \to e+p+\rho$ or ω, much as the virtual Compton cross section is separated out in inclusive electroproduction. We may use (4.63) for virtual ω photoproduction, but (4.62) must be multiplied by $\mathfrak{F}(q_1^2, m_\rho^2)$ to obtain the virtual ρ photoproduction amplitude. In both cases q_1^2 is spacelike.

V. ADLER SUM RULE

In this section, we briefly discuss the role of the Adler sum rule[19] in our model. We denote the amplitude $T_{2V}^{\bar{\nu}p} - T_{2V}^{\nu p}$ by $T_{2V}^{(-)}$, which has $I=1$ in the t channel and is odd under s-u crossing. In the scale-invariant limit, the Adler sum rule for the vector current may be written, in an obvious notation, as

$$\int_0^1 \frac{dx}{x} F_{2V}^{(-)}(x) = 1, \tag{5.1}$$

where $x = 1/\omega$.

The Pomeron does not contribute to $T_{2V}^{(-)}$, and for *pure Regge behavior* the dominant high-energy contribution should be given by the ρ Regge pole. In our model, the ρ trajectory has intercept $\alpha_\rho(0) = \frac{1}{2}$, so that

$$T_{2V}^{(-)}(\nu, q^2) = O(\nu^{-3/2}) \text{ for large } |\nu| . \tag{5.2}$$

Therefore, provided that $T_{2V}^{(-)}$ is analytic, it satisfies an unsubtracted dispersion relation

$$T_{2V}^{(-)}(\nu, q^2) = \frac{2\nu}{\pi} \int_{\nu_t}^\infty \frac{d\nu'}{\nu'^2 - \nu^2} \operatorname{Im} T_{2V}^{(-)}(\nu', q^2), \tag{5.3}$$

where ν_t is the inelastic threshold. By using (5.2), we may derive from (5.3) the superconvergence relation

$$\int_{\nu_t}^\infty d\nu \operatorname{Im} T_{2V}^{(-)}(\nu, q^2) = 0 . \tag{5.4}$$

In the scale-invariant limit this may be written as

$$\int_0^1 \frac{dx}{x} F_{2V}^{(-)}(x) = 0, \tag{5.5}$$

which contradicts (5.1). Thus the pure Regge term does not contribute to the sum rule (5.1).

Because it is analytic and has the asymptotic behavior (5.2), our model for $A_V^{(\bar{\nu},\nu)}$, defined in (2.27), leads to the result (5.5). However, we require that the full amplitude $T_{2V}^{(-)}$ must satisfy the Dashen–Fubini–Gell-Mann[12] sum rule

$$\int_{s_t}^\infty ds \operatorname{Im} T_{2V}^{(-)}(s, t, q_1^2, q_2^2) = 4\pi M F_V(t), \tag{5.6}$$

or, equivalently,

$$\lim_{s\to\infty} T_{2V}^{(-)}(s, t, q_1^2, q_2^2) = -\frac{8MF_V(t)}{s} . \tag{5.7}$$

When we fix $q_1^2 = q_2^2 = q^2$ and $t=0$, and take the scale-invariant limit, (5.6) reduces to

$$\int_0^1 \frac{dx}{x} F_{2V}^{(-)}(x) = 1, \tag{5.1}$$

which is the Adler sum rule. It is well known[16,20] that the Dashen–Fubini–Gell-Mann sum rule may be satisfied by a fixed pole at $J=1$ in the angular momentum plane, and it is the fixed pole term F in (2.27) which reinstates the Adler sum rule. As an illustrative model for the fixed-pole contribution, we take

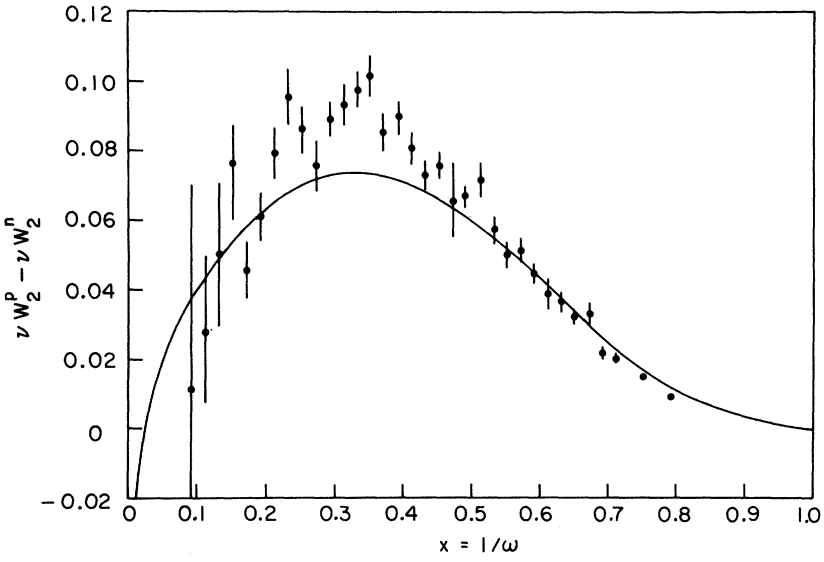

FIG. 2. The difference $F_2^p - F_2^n$ plotted versus x; the data are from Ref. 3, and the solid line is our fit.

$$F^{(\bar{\nu},\nu)}(s,t,q_1^2,q_2^2)=\pm 4M\left[\frac{F_V(q_1^2)F_V(q_2^2)}{M^2-s}-\frac{F_V(q_1^2)F_V(q_2^2)-1/2F_V(t)}{(a+b(q_t^2-q_1^2)^{1/4}(q_t^2-q_2^2)^{1/4}+(s_t-s)^{1/2})^2}\right]-(s\rightarrow u), \quad (5.8)$$

where a and b are positive constants. The model (5.8) has the following properties:

(i) It is antisymmetric under $s \rightarrow u$.

(ii) For q_1^2 and q_2^2 in the first sheet, it is analytic in q_1^2 and q_2^2 except for cuts in the region $q_t^2 \leq q_1^2 < \infty$, $q_t^2 \leq q_2^2 < \infty$. It is analytic in s on the physical sheet, except for poles and cuts on the real s axis.

(iii) The gauge condition (2.28) is satisfied by (5.8).

(iv) The Dashen–Fubini–Gell-Mann sum rule (5.6) is satisfied.

(v) In the scale-invariant limit, the contribution of (5.8) to the structure function $F_{2V}^{(-)}(x)$ is given by

$$F_{2V}^{(-)}(x)_{\text{fixed pole}}=\frac{2b}{\pi}\frac{x^{1/2}(1-x)^{1/2}}{(1+b^2x-x)^2}. \quad (5.9)$$

This function satisfies the Adler sum rule (5.1).

Because the fixed pole does not occur in the Compton amplitude, we feel that $F_2^{\bar{\nu}p}-F_2^{\nu p}$ and $F_2^{\bar{\nu}p}/F_2^{\nu p}$ may bear little resemblance to the electroproduction structure functions $F_2^p-F_2^n$ and F_2^p/F_2^n, respectively. Therefore, one cannot draw conclusions about the validity of the Adler sum rule from the threshold behavior of F_2^p and F_2^n.[21]

VI. COMPARISON WITH EXPERIMENT

In the following, we confront our model with experimental data on structure functions and cross sections.

(1) Structure functions for electroproduction. To begin, we assume that the electroproduction structure functions νW_2^p and νW_2^n have already reached their scale-invariant limits F_2^p and F_2^n, within a few percent, for $-q^2 \gtrsim 2$ (GeV/c)^2. We then fit the preliminary SLAC-MIT data,[3] subject to the constraints (4.18) and (4.21). Without loss of generality, we may fix $B_P=B_N=B_{1N}=B_{2N}=-1$. The A_2 and A_2' contributions are fixed by fitting the data for the proton-neutron difference $\Delta F_2=F_2^p-F_2^n$, using the form (4.47). With the values $\gamma_{A_2}=-0.462$, $A_{1N}=5.8$, $C_{1N}=9.0$, $\gamma_{A_2'}=0.175$, $A_{2N}=2.99$, and $C_{2N}=3.0$, we obtain the fit shown in Fig. 2. It should be noted that, because of the superconvergence property of the Regge terms in our model, ΔF_2 must pass through zero at least once. In fact, our fit in Fig. 2 is negative in the region $\omega \gtrsim 40$ or $x \lesssim 0.025$.

The fit to the ratio F_2^n/F_2^p, shown in Fig. 3, determines the parameters for the Pomeron and P' in (4.47); they are given by $\gamma_P=0.17$, $A_P=1.0001$, $C_P=0.52$, $\gamma_{P'}=0.29$, $A_N=2.08$, and $C_N=2.11$. The resulting scale-invariant proton and deuteron structure functions are compared with the data in Fig. 4, and the individual contributions of the Pomeron, P', and (A_2+A_2') terms are shown in Fig. 5. Although each of the contributing terms has square-root threshold behavior which does not agree with the data, they combine to produce threshold behavior which is closer to the $(\omega-1)^3$ suggested by the Bloom-Gilman[22] sum rule. With the choice of parameters given above, there is a positivity violation in F_2 for $1 \leq \omega \lesssim 1.0001$ because the Pomeron term is negative in that region. This violation is connected to unitarity, and in principle our model could be unitarized[23] to remove it, although such a program is beyond the scope of the present work.

(2) Compton scattering and neutrino scattering. The proton-neutron difference $\Delta\sigma=\sigma(\gamma p)-\sigma(\gamma n)$ is given by

$$\Delta\sigma=2(\sigma_{A_2}+\sigma_{A_2'}), \quad (6.1)$$

where σ_{A_2} and $\sigma_{A_2'}$ are defined in (4.54). Provided we neglect the resonances and satellites, this is

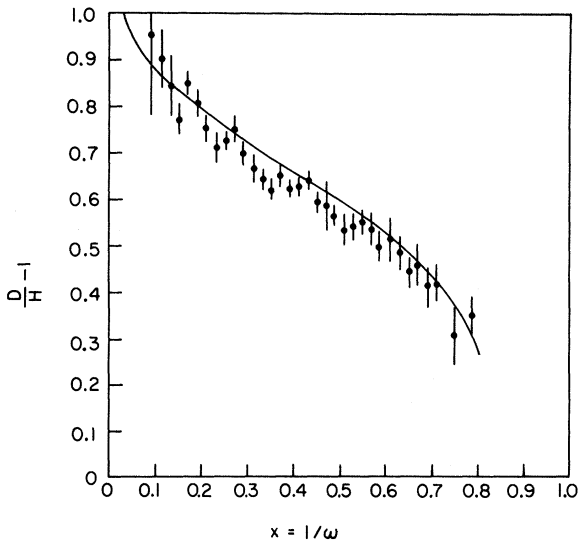

FIG. 3. The ratio F_2^n/F_2^p plotted versus x; the data are from Ref. 3, and the solid line is our fit.

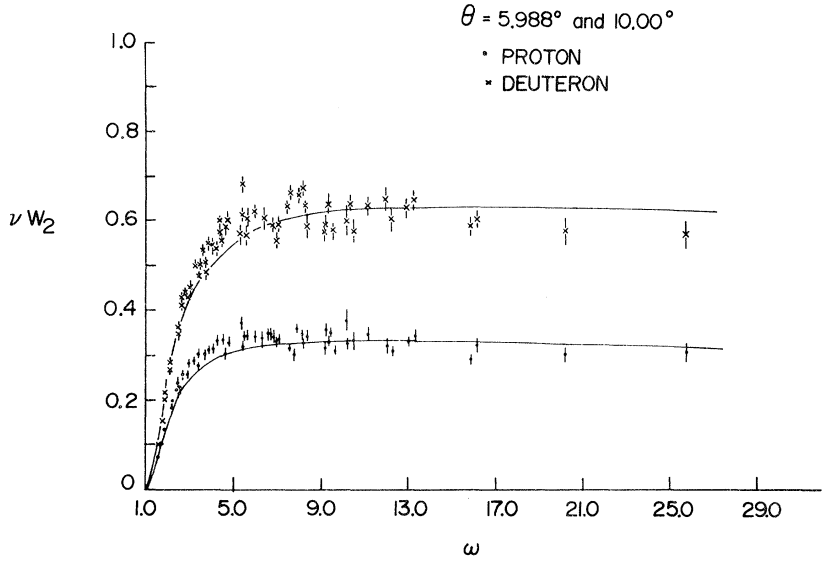

FIG. 4. The scale-invariant proton and deuteron structure functions plotted versus ω. The data are from Ref. 3, and the solid lines are out fits.

determined from ΔF_2 once the scale-breaking parameter $(a+q_t)$ is fixed. The fit to the data[24] in Fig. 6 is obtained with $(a+q_t)^2 = 1.24$ (GeV/c)^2. Now, in principle, the Compton residues γ_{Pc} and $\gamma_{P'c}$ could be determined by a fit to the total photoabsorption cross section, which would then predict the neutrino combination $(F_{2V}^{\bar{\nu}p} + F_{2V}^{\nu p})$ given in (4.53). In practice, the Compton data are not precise enough for a prediction; therefore, we include the preliminary neutrino data[14] as input. In particular, we require $(F_{2V}^{\bar{\nu}p} + F_{2V}^{\nu p})$ to tend smoothly to zero near threshold, as the electroproduction structure functions do, and furthermore the value of $\int (F_{2V}^{\bar{\nu}p}(x) + F_{2V}^{\nu p}(x))\,dx$ should agree with experiment.

By determining the Compton residues γ_{Pc} and $\gamma_{P'c}$, and combining (4.59) with (4.52), the residues γ_P^{33} and $(\gamma_{1\rho}^{33} + 2\gamma_{2\rho}^{33})$, which appear in the neutrino-scattering structure function (4.53), may be determined. With the values $\gamma_{Pc} = 2.66$ GeV^{-3} and $\gamma_{P'c} = 4.52$ GeV^{-3} as well as $m_\rho = 760$ MeV, $\Gamma_\rho = 120$ MeV, $m_\omega = 784$ MeV, and $\Gamma_\omega = 10$ MeV,[25] we obtain the fit to the total photon-proton cross section data,[24,26] shown in Fig. 7, and the asymptotic behavior displayed in Fig. 8. We restrict our fits to $\nu \geq 7$ GeV because we have neglected resonances which become important for $\nu < 7$ GeV. Simultaneously, we obtain the neutrino-scattering structure function shown in Fig. 9. It has the correct threshold behavior, and

$$\int_0^1 (F_{2V}^{\bar{\nu}p}(x) + F_{2V}^{\nu p}(x))\,dx = 0.484\,. \tag{6.2}$$

If we assume CVC and chiral symmetry[14,27]

$$F_{2V}^{(\bar{\nu},\nu)}(x) = F_{2A}^{(\bar{\nu},\nu)}(x)\,, \tag{6.3}$$

then

$$\int_0^1 (F_2^{\bar{\nu}p}(x) + F_2^{\nu p}(x))\,dx = 0.968\,, \tag{6.4}$$

which is consistent with the experimental value[14] 0.98 ± 0.14.

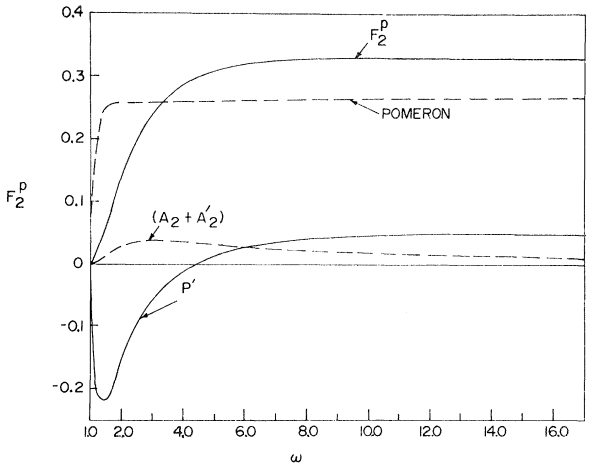

FIG. 5. The proton structure function F_2^p along with the Pomeron, P', and $(A_2 + A_2')$ contributions given by (4.47) plotted versus ω.

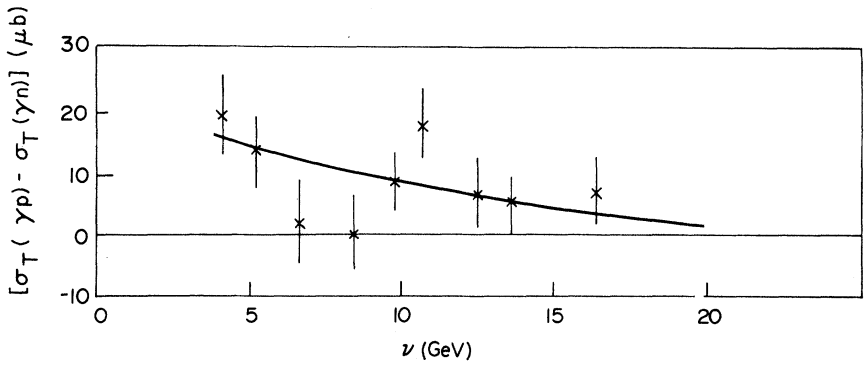

FIG. 6. The difference $\sigma(\gamma p) - \sigma(\gamma n)$ for physical photons plotted versus the photon energy E in the Regge region. The data are from Ref. 24, and the solid line is our fit.

Our results are quite sensitive to variations in m_ρ, Γ_ρ, m_ω and Γ_ω when the other parameters are held constant. The reason is that for values of m_ρ and Γ_ρ, which are consistent with experiment, the propagators $D_3(0)$ and $D_8(0)$ are nearly equal, and the isovector and isoscalar parts are not strongly differentiated in (4.59). However, provided that $D_3(0) \neq D_8(0)$, it is still possible to obtain simultaneous fits to the photoabsorption and neutrino scattering data by varying the parameters γ_{Pc} and $\gamma_{P'c}$ slightly.

(3) Compton differential cross section. To apply the Compton amplitude (4.60) to nonforward scattering, we need to know the trajectories $\alpha_P(t)$ and $\alpha_\rho(t)$. In (4.22), we take $b_P = 0.3$ (GeV/c)$^{-2}$ and $\Delta_P = 10^4$ (GeV/c)^2, so that for small $|t|$, b_P is the slope of an effectively linear Pomeron trajectory. Similarly we choose $\Delta_\rho = 10^4$ (GeV/c)^2 in (4.24). We also take $c_\rho = 0.1$ (GeV/c)$^{-1}$ and require that $\alpha_\rho(0) = \frac{1}{2}$ and $\alpha_\rho(m_\rho{}^2) = 1$, which fixes a_ρ and b_ρ. Aside from the parameters g_P, $g_{P'}$, and g_{A_2}, the amplitude (4.60) is now determined. With the values $g_P = 7.0$, $g_{P'} = -0.5$, and $g_{A_2} = 3.0$, we obtain the fits to the Compton differential cross section data[28] shown in Fig. 10, and for the near-forward scattering shown in Fig. 11. Note that our fits display the slight shrinkage of the diffraction peak inherent in a Regge-pole model.

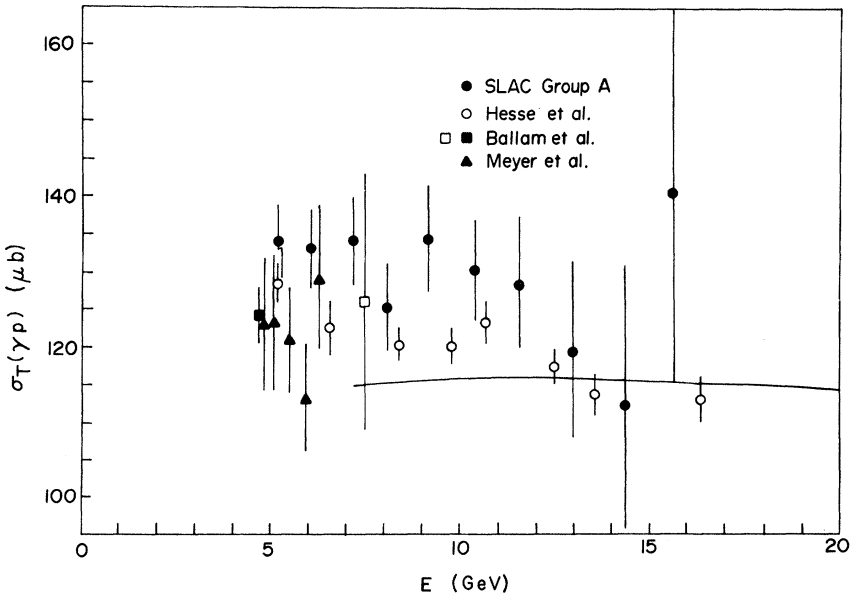

FIG. 7. The total photon-proton cross section for physical photons plotted versus the photon energy E in the Regge region. The solid line is our fit and the data are from Refs. 24 and 26.

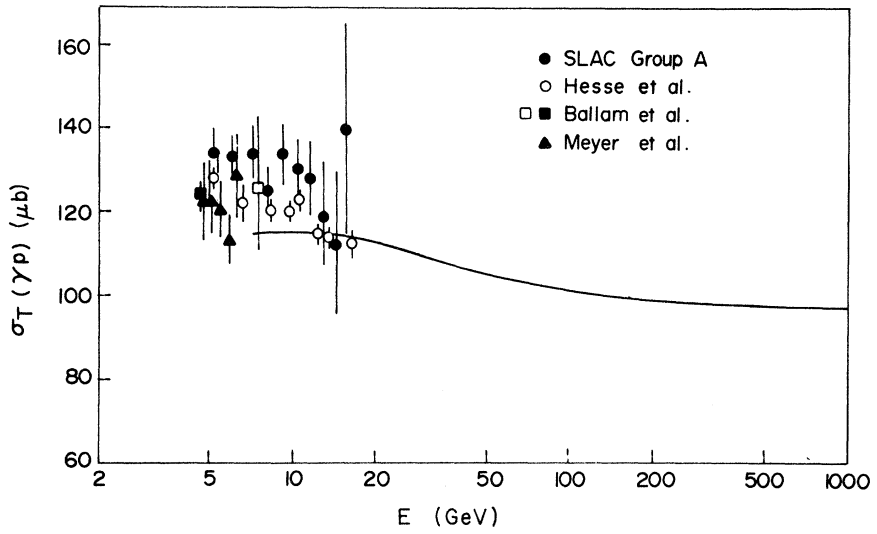

FIG. 8. The same data and the same fit as in Fig. 7, plotted to display the predictions of our fit up to $E = 1000$ GeV.

(4) Scale breaking. We neglect the resonances and satellites in (4.42) to fit the scale-breaking behavior[2] of νW_2. Figure 12 shows our fit for νW_2 vs $-q^2$ at fixed values of ω, and for $\nu \geq 5$ GeV. We do not feel justified in attempting to describe the data for $\nu < 5$ GeV for, as in Compton scattering, the resonance contribution is significant at low

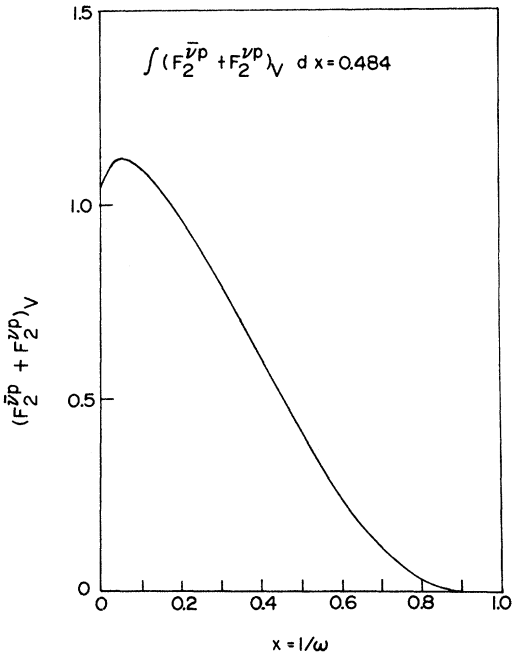

FIG. 9. The neutrino-scattering structure function $F_{2\bar{\nu}}^{\bar{\nu}p} + F_{2\nu}^{\nu p}$ plotted versus x.

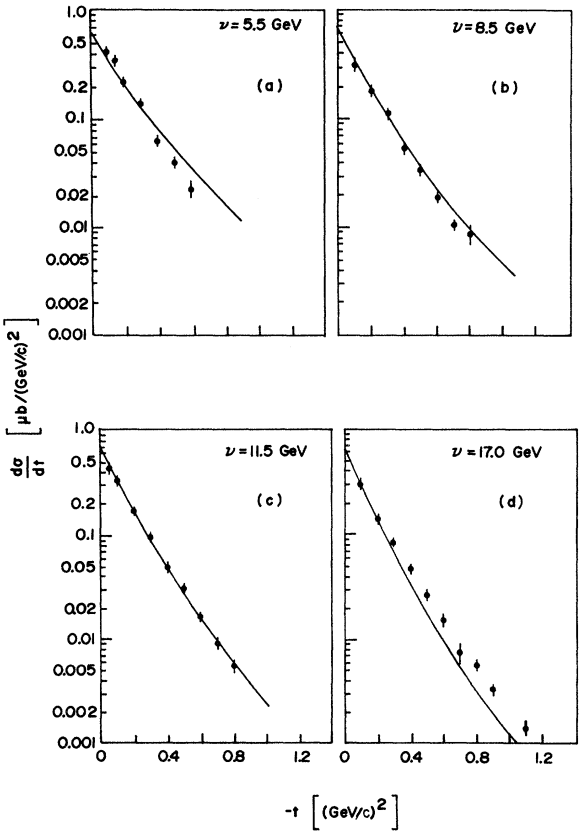

FIG. 10. The differential cross section $d\sigma/dt$ for p-γ scattering plotted versus $-t$. Four values of lab energy ν are shown: (a) 5.5, (b) 8.5, (c) 11.5, (d) 17 GeV. The solid line is our fit and the data are from Ref. 28.

energy. For the parameters defined in (4.33), we get $n=6$, $c=4.1$ (GeV/c)^2, and $a=0.12$ GeV/c.

(5) Vector-meson photoproduction. Once the vector-meson–photon coupling constants are given, the ρ- and ω-photoproduction amplitudes (4.62) and (4.63), respectively, are fully determined. We use the latest storage-ring values,[29]

$$f_\rho{}^2/4\pi = 2.56 \pm 0.27, \qquad (6.5)$$
$$f_\omega{}^2/4\pi = 19.2 \pm 2.0,$$

to obtain the *parameter-free* predictions for the ρ^0 photoproduction data[30,31] shown in Fig. 13, and for the ω photoproduction data[32] shown in Fig. 14.

Both the normalization and slope of the ρ^0 photoproduction predictions are consistent with experiment. The ω photoproduction prediction is consistent with the data, at 9.3 GeV, but falls slightly below the data for 4.7 and 7.5 GeV, possibly reflecting the fact that we have neglected the pion, which may be exchanged in the t channel. The pion is expected to contribute to the energy dependence of the differential cross section at low energy, but because $\alpha_\pi(0)<0$, it should not be too important for $\nu>5$ GeV.

(6) Virtual photoproduction. In Fig. 15, we show our prediction for the ρ^0 meson virtual photoproduction differential cross section data[33] for three values of q^2, the (mass)^2 of the virtual photon at a c.m. energy $W=2.5$ GeV. We also show our prediction for the real photoproduction data[31,34] at $W=2.48$ GeV. Of special interest is the q^2 dependence, which is consistent with the data. Figure 16 shows the comparison of our prediction with the latest data[35] for the q^2 dependence of $\sigma_\rho(W,q^2)/\sigma_{\rm tot}(W,q^2)$, where $\sigma_\rho(W,q^2)$ is the cross section for ρ^0 production and

$$\sigma_{\rm tot}(W,q^2)=\sigma_T(W,q^2)+\epsilon\sigma_S(W,q^2). \qquad (6.6)$$

Here, the polarization parameter ϵ is the ratio of longitudinal to transverse polarization of the virtual photons. Since ϵ is near unity and $\sigma_S \lesssim 0.2\sigma_T$, we may approximate (6.6) by

$$\sigma_{\rm tot}(W,q^2)=\sigma_T(W,q^2)+\sigma_S(W,q^2), \qquad (6.7)$$

which is given by (2.38). To obtain σ_ρ we integrate $d\sigma_\rho/dt$ for $-t \leq 3.0$ (GeV/c)^2. Our model is not expected to be applicable for $|t|>3.0$ (GeV/c)^2 because only two of the invariant amplitudes are retained in our treatment; however, since the differential cross section falls off rapidly for large $|t|$, contributions from this region are probably small. The error bars in Fig. 16 do not show the estimated 16% systematic uncertainty[35] in $\sigma_\rho/\sigma_{\rm tot}$; the photoproduction data are taken from Ref. 36. The prediction is made for $W=5.0$ GeV, and is consistent with all data points except the one for the highest value of $|q^2|$.

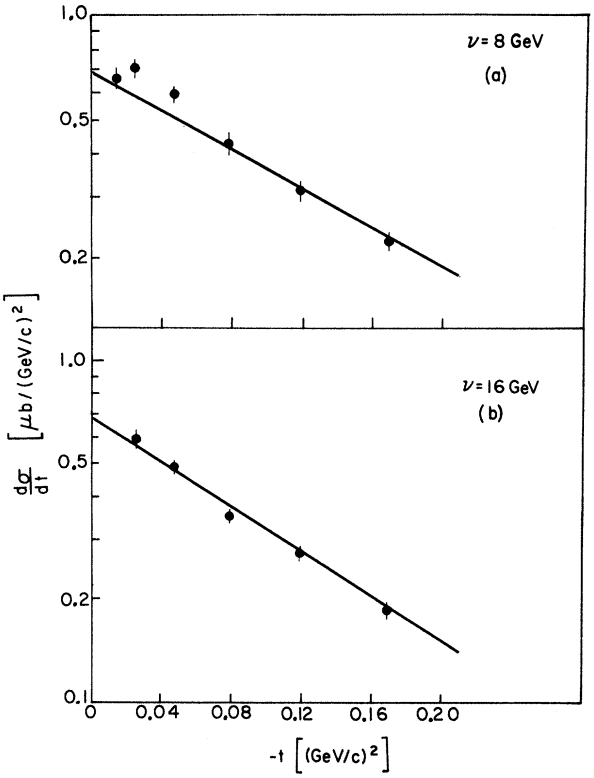

FIG. 11. $d\sigma/dt$ plotted versus $-t$ for small values of $-t$. The solid lines are our fits and the data are from Ref. 28. The lab energies are (a) 8, (b) 16 GeV.

For completeness, in Fig. 17 we show our prediction for the q^2 dependence of $\sigma_{\rm tot}$ given by (6.7). The data are from Ref. 37, and we have taken $W=3.5$ GeV.

VII. CONCLUSIONS

We have constructed a model for current-hadronic interactions which possesses Mandelstam analyticity, crossing symmetry, scale invariance, vector dominance, Regge behavior, and resonances. The model is "unified" in that it is applicable to several processes over a broad range in s, t, $q_1{}^2$, and $q_2{}^2$. It gives good fits to electroproduction, neutrino scattering, and Compton data in the high-energy region, as well as predictions for vector-meson photoproduction and electroproduction, which are also consistent with experiment.

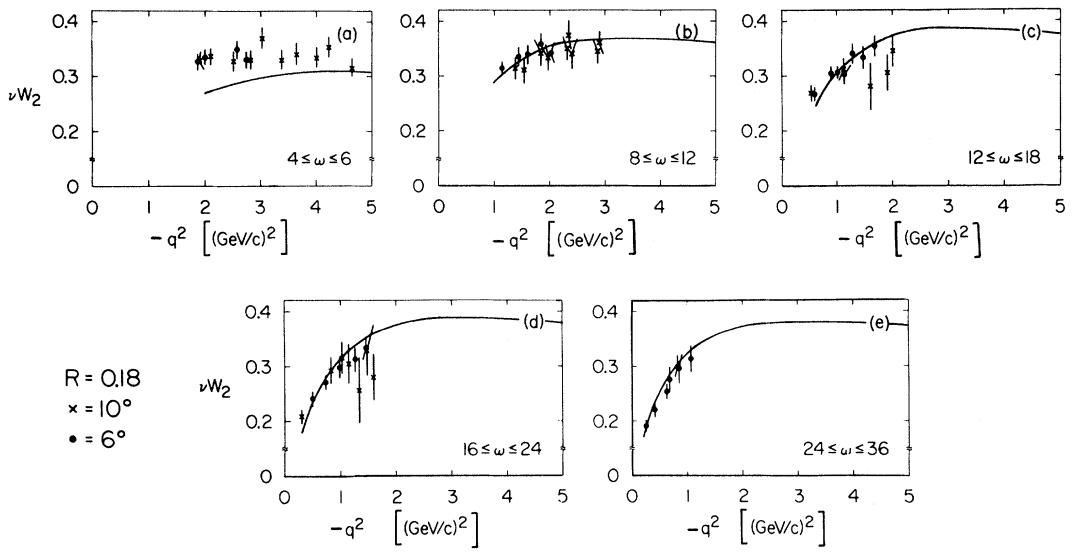

FIG. 12. The proton structure function νW_2^p plotted versus $(-q^2)$ for fixed ω showing the scale invariance breaking. Each graph has ω restricted to a narrow range, and the energy is restricted to $\nu \geq 5$ GeV. We have chosen the average value of ω in each case to fit the data in Ref. 2.

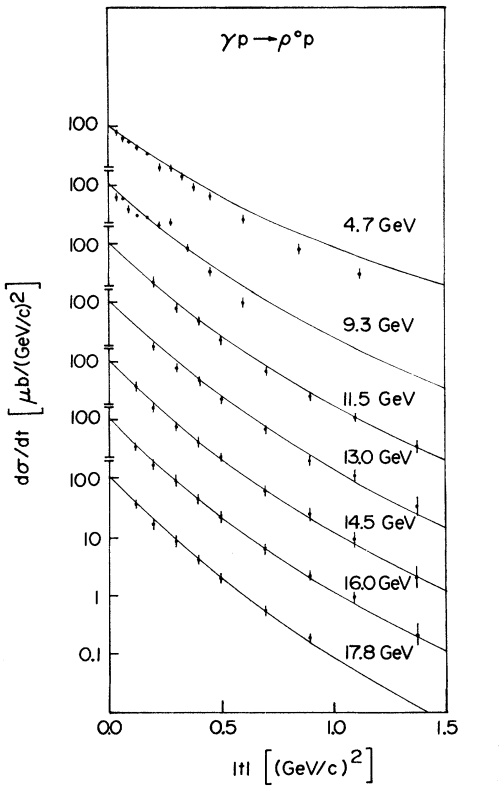

FIG. 13. The ρ^0 photoproduction differential cross section plotted versus $|t|$ for lab energies between 4.7 and 17.8 GeV. The solid lines are our predictions for the data from Refs. 30 and 31.

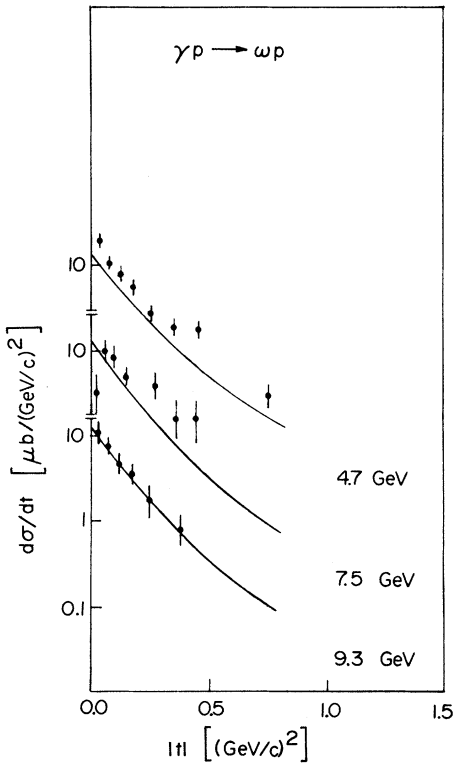

FIG. 14. The ω photoproduction differential cross section plotted versus $|t|$ at 4.7, 7.5, and 9.3 GeV. The data are from Ref. 32, and the solid lines are our predictions.

Because of unitarity violations, we have not used the data to test the low-energy, resonance-dominated behavior of our amplitude, although this can in practice be rectified. Another possible drawback is the omission of the ϕ meson from our vector dominance assumption; the ϕ is expected to contribute to processes involving isoscalar currents, but there is nothing, in principle, that prevents us from including it in the model.

The threshold behavior of our model requires some comment. The fit to the scale-invariant electroproduction structure function, shown in Fig. 4, results from the sum of the Pomeron and Regge terms. Figure 5 shows that our Regge terms have threshold behavior; for instance, the Pomeron contribution is not the constant function one would obtain from a "pure" Regge form, and it is this which allows us to fit the structure function down to $\omega = 1$. In contrast to some models,[6] in which the threshold behavior is put in by hand, our threshold behavior does not disappear as $q^2 \to 0$,

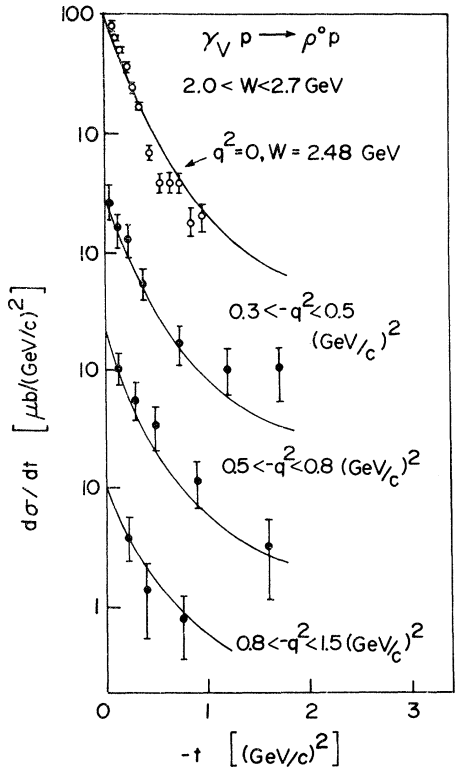

FIG. 15. The ρ^0 virtual photoproduction differential cross section plotted versus $-t$. The data from Ref. 33 (closed circles) are shown for $2.0 < \omega < 2.7$ GeV and for various values of $(-q^2)$. The solid lines are our predictions for $W = 2.5$ GeV and values of $(-q^2)$ in the mid-range of the experimental values. The photoproduction data from Refs. 31 and 34 for $W = 2.48$ GeV are shown as open circles and the solid line is our prediction.

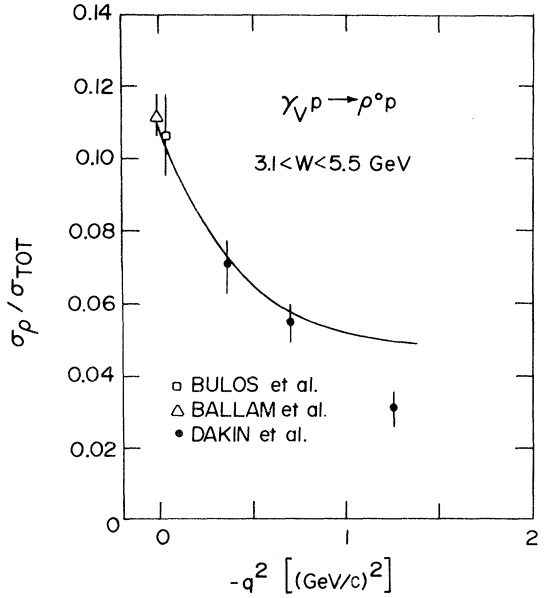

FIG. 16. The ratio $\sigma_\rho(W, q^2)/\sigma_{tot}(W, q^2)$ plotted versus $-q^2$. The virtual photoproduction data (closed circles) are shown for $3.1 < W < 5.5$ GeV and are from Ref. 35. The error bars do not include the systematic error in the data. The real photoproduction data are for $4.2 < W < 5.0$ GeV and are from Ref. 36. The solid line is our prediction for $W = 5.0$ GeV.

and for physical Compton scattering the properly unitarized resonances must contribute significantly at low energy.

To check the generality of our results, it would be interesting to have more data for inclusive neutrino scattering, and also for processes involving photons which are even farther off-mass-shell than those currently available.

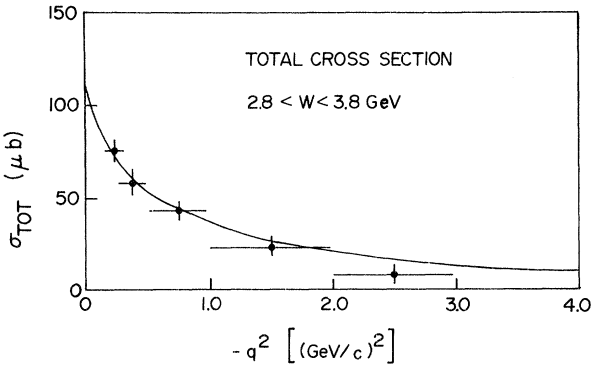

FIG. 17. The total virtual Compton cross section plotted versus $-q^2$. The data, from Ref. 37, are for W between 2.8 and 3.8 GeV. The solid line is our prediction for $W = 3.5$ GeV.

*Work supported in part by the National Research Council of Canada.

[1]J. D. Bjorken, Phys. Rev. 179, 1547 (1969).

[2]E. D. Bloom *et al.*, MIT-SLAC Report No. SLAC-PUB-796, 1970 (unpublished), presented at The Fifteenth International Conference on High Energy Physics, Kiev, U. S. S. R., 1970.

[3]H. W. Kendall, in *Proceedings of the 1971 International Symposium on Electron and Photon Interactions at High Energies,* edited by N. B. Mistry (Laboratory of Nuclear Studies, Cornell University, Ithaca, New York, 1972), p. 248; A. Bodek *et al.*, Phys. Rev. Lett. 30, 1087 (1973).

[4]R. P. Feynman, Phys. Rev. Lett. 23, 1415 (1969); S. D. Drell, D. J. Levy, and T.-M. Yan, *ibid.* 22, 744 (1969); J. D. Bjorken and E. Paschos, Phys. Rev. 185, 1975 (1969); P. Landshoff and J. C. Polkinghorne, Nucl. Phys. B28, 240 (1971); J. Kuti and V. F. Weisskopf, Phys. Rev. D 4, 3418 (1971).

[5]K. Wilson, Phys. Rev. 179, 1499 (1969); H. Fritzsch and M. Gell-Mann, in *Broken Scale Invariance and the Light Cone,* 1971 Coral Gables Conference on Fundamental Interactions at High Energy, edited by M. Dal Cin, G. J. Iverson, and A. Perlmutter (Gordon and Breach, New York, 1971), Vol. 2, p. 1, and in *Proceedings of the International Conference on Duality and Symmetry in Hadron Physics,* edited by E. Gotsman (Weizman Science Press, Jerusalem, 1971); R. Jackiw, R. Van Royen, and G. B. West, Phys. Rev. D 2, 2473 (1970).

[6]J. W. Moffat and V. G. Snell, Phys. Rev. D 3, 2848 (1971); 4, 1452 (1971). See also J. W. Moffat, in *Proceedings of the Eleventh Internationale Universitätswochen für Kernphysik, Schladming, Austria,* edited by P. Urban (Springer, New York 1972).

[7]R. A. Brandt, Phys. Rev. Lett. 22, 1149 (1969); H. R. Pagels, Phys. Lett. 34B, 299 (1971); Phys. Rev. D 3, 1217 (1971).

[8]R. C. Brower and J. H. Weis, Phys. Rev. 188, 2486 (1969); 188, 2495 (1969); P. V. Landshoff and J. C. Polkinghorne, Nucl. Phys. B19, 432 (1970).

[9]J. J. Sakurai, Phys. Rev. Lett. 22, 981 (1969); C. F. Cho, G. J. Gounaris, and J. J. Sakurai, Phys. Rev. 186, 1734 (1969); K. Fujikawa, Phys. Rev. D 4, 2794 (1971).

[10]J. W. Moffat, Phys. Rev. D 3, 1222 (1971).

[11]P. Curry, I. O. Moen, J. W. Moffat, and V. Snell, Phys. Rev. D 3, 1233 (1971).

[12]R. Dashen and M. Gell-Mann, Phys. Rev. Lett. 17, 340 (1966); S. Fubini, Nuovo Cimento 43, 475 (1966).

[13]J. W. Moffat and A. C. D. Wright, Phys. Rev. D 5, 75 (1972).

[14]G. Myatt and D. H. Perkins, Phys. Lett. 34B, 542 (1971); D. H. Perkins, in *Proceedings of the XVI International Conference on High Energy Physics, Chicago-Batavia, Ill., 1972,* edited by J. D. Jackson and A. Roberts (NAL, Batavia, Ill., 1973), Vol. 4, p. 189.

[15]W. A. Bardeen and W.-K. Tung, Phys. Rev. 173, 1423 (1968).

[16]J. B. Bronzan, I. S. Gerstein, B. W. Lee, and F. E. Low, Phys. Rev. 157, 1448 (1967).

[16a]Throughout our work the proton is treated as spinless, that is, the average over proton spins is taken before squaring the amplitude. When the spin of the proton is taken into account there is a contribution to the unpolarized differential cross section in addition to (2.33). However, the spinless approximation should be satisfactory at high energy and small t. For a discussion of this point in the forward direction see M. Damashek and F. J. Gilman, Phys. Rev. D 1, 1319 (1970), and also papers quoted in Ref. 6.

[17]P. Curry and J. W. Moffat, Phys. Rev. 184, 1885 (1969).

[18]H. Fraas and D. Schildknecht, Nucl. Phys. B14, 543 (1969); C. Driver *et al.*, Nucl. Phys. B38, 1 (1972).

[19]S. L. Adler, Phys. Rev. 143, 1144 (1966).

[20]J. B. Bronzan, I. S. Gerstein, B. W. Lee, and F. E. Low, Phys. Rev. Lett. 18, 32 (1967); V. Singh, *ibid.* 18, 36 (1967).

[21]J. D. Bjorken and S. F. Tuan, Comments Nucl. Part. Phys. 5, 71 (1972); J. J. Sakurai, H. B. Thacker, and S. F. Tuan, Nucl. Phys. B48, 353 (1972); S. F. Tuan, Phys. Rev. D 7, 2092 (1973).

[22]E. D. Bloom and F. J. Gilman, Phys. Rev. Lett. 25, 1140 (1970).

[23]J. W. Moffat and B. Weisman, Phys. Rev. D 6, 238 (1972). In this work, approximately unitary solutions are obtained for the "parent" model of Refs. 10 and 11 for $\pi\pi$ and $K\pi$ scattering at low energy.

[24]W. P. Hesse *et al.*, Phys. Rev. Lett. 25, 613 (1970).

[25]Particle Data Group, Rev. Mod. Phys. 45, S1 (1973).

[26]E. D. Bloom *et al.*, SLAC Report No. SLAC-PUB 653 (unpublished); D. O. Caldwell *et al.*, Phys. Rev. Lett. 23, 1256 (1969); H. Meyer *et al.*, DESY reports, 1969 (unpublished); J. Ballam *et al.*, Phys. Rev. Lett. 21, 1544 (1968); 23, 498 (1969).

[27]J. D. Bjorken and E. A. Paschos, Phys. Rev. D 1, 3151 (1970).

[28]R. L. Anderson *et al.*, Phys. Rev. Lett. 25, 1218 (1970); G. Buschhorn *et al.*, Phys. Lett. 33B, 241 (1970); A. M. Boyarski *et al.*, Phys. Rev. Lett. 26, 1600 (1971).

[29]G. Wolf, in *Proceedings of the 1971 International Symposium on Electron and Photon Interactions at High Energies,* edited by N. B. Mistry (Laboratory of Nuclear Studies, Cornell University, Ithaca, New York, 1972); P. Söding, in Proceedings of the Topical Seminar on Electromagnetic Interactions, Trieste, 1971 (unpublished); D. Schildknecht, in *Springer Tracts in Modern Physics,* edited by G. Höhler (Springer, New York, 1972), Vol. 63, p. 57; J. Lefrancois, in *Proceedings of the 1971 International Symposium on Electron and Photon Interactions at High Energies,* edited by N. B. Mistry (Laboratory of Nuclear Studies, Cornell University, Ithaca, New York, 1972).

[30]H. H. Bingham *et al.*, Phys. Rev. Lett. 24, 955 (1970); 24, 960 (1970); J. Ballam *et al.*, in *Proceedings of the 1971 International Symposium on Electron and Photon Interactions at High Energies,* edited by N. B. Mistry (Laboratory of Nuclear Studies, Cornell University, Ithaca, New York, 1972); K. C. Moffeit, thesis, LBL Report No. UCRL-19890, 1970 (unpublished); R. Anderson *et al.*, Phys. Rev. D 1, 27 (1970).

[31]J. Ballam *et al.*, Phys. Rev. D 5, 545 (1972).

[32]ABBHHM Collaboration, Phys. Rev. 175, 1669 (1968); Y. Eisenberg *et al.*, Phys. Lett. 34B, 439 (1971); J. Ballam *et al.*, Phys. Rev. Lett. 24, 1364 (1970), and SLAC Report No. SLAC-PUB 980, 1971 (unpublished); W. J. Podolsky, thesis, LBL Report No. UCRL-20128, 1971 (unpublished).

[33]V. Eckardt *et al.*, in *Proceedings of the XVI International Conference on High Energy Physics, Chicago-Batavia,*

Ill., 1972, edited by J. D. Jackson and A. Roberts (NAL, Batavia, Ill., 1973).
[34]K. C. Moffeit *et al.*, Phys. Rev. D 5, 1603 (1972).
[35]J. T. Dakin *et al.*, Phys. Rev. D 8, 687 (1973).
[36]J. Ballam *et al.*, *ibid.* 7, 3150 (1973); F. Bulos *et al.*, in *Proceedings of the XVI International Conference on High Energy Physics, Chicago-Batavia, Ill., 1972,* edited by J. D. Jackson and A. Roberts (NAL, Batavia, Ill., 1973).
[37]J. Ballam *et al.*, SLAC Report No. SLAC-PUB 1163, 1972 (unpublished).